# RIF1 integrates DNA repair and transcriptional requirements during the establishment of humoral immune responses

Ali Rahjouei[1#], Eleni Kabrani[1#], Maria Berruezo-Llacuna[1,2], Robert Altwasser[1,3], Veronica Delgado-Benito[1], Rushad Pavri[4], and Michela Di Virgilio[1,5,*]

[1]Laboratory of Genome Diversification & Integrity, Max Delbrück Center for Molecular Medicine in the Helmholtz Association, Berlin 13125, Germany

[2]Humboldt-Universität zu Berlin, Berlin 10117, Germany

[3]Current address: Department of Hematology, Oncology, and Cancer Immunology, Charité-Universitätsmedizin Berlin, Berlin 10117, Germany

[4]Research Institute of Molecular Pathology (IMP), 1030 Vienna, Austria

[5]Charité-Universitätsmedizin Berlin, Berlin 10117, Germany

[#]These authors contributed equally

*Correspondence: michela.divirgilio@mdc-berlin.de

**Abstract**

The establishment of protective immune responses relies on the ability of terminally differentiated B cells to secrete a broad variety of antigen-specific antibodies with different effector functions. RIF1 is a multifunctional protein that promotes antibody isotype diversification *via* its DNA end protection activity during class switch recombination (CSR). In this study, we showed that RIF1 ablation resulted in increased plasmablast (PB) formation *ex vivo* and enhanced terminal differentiation into plasma cells (PCs) upon immunization. Mechanistically, this phenotype is independent from RIF1's role in DNA repair and CSR, and reflects its ability to modulate the transcriptional status of a subset of BLIMP1 target genes. Therefore, in addition to promoting antibody isotype diversification, RIF1 fine-tunes the kinetics of late B cell differentiation, thus providing an additional layer of control in the establishment of humoral immunity.

## Introduction

During early B cell development in the bone marrow, common lymphoid progenitors develop into immature B cells *via* a step-wise process linked to the rearrangement of their antibody receptor/immunoglobulin (Ig) genes by V(D)J recombination [1,2]. Immature B cells expressing a functional and non-autoreactive B cell receptor (BCR) migrate to the periphery, where they complete their maturation into quiescent resting cells [1,2]. The encounter of these naïve mature B cells with their cognate antigen in secondary lymphoid organs triggers late B cell differentiation into effector cells, often accompanied by further BCR/Ig diversification *via* somatic hypermutation (SHM) and class switch recombination (CSR) [3]. SHM and CSR provide the molecular bases for generating high-affinity and isotype-switched BCRs/Igs, respectively [4]. At the cellular level, the combined effect of BCR engagement, helper T and follicular dendritic cell-derived signals induces the formation of specialized microstructures known as germinal centers (GCs), where activated B cells undergo a major proliferative burst, selection of high-affinity BCR variants, and differentiation into either antibody-secreting cells (ASCs, plasmablasts (PBs) and plasma cells (PCs)) or memory B cells [5]. B cell activation can also lead to PB generation at extrafollicular sites, which are also characterized by B cell proliferation and represent the main source of ASCs in T-cell independent responses [6]. BLIMP1 (encoded by the *Prdm1* gene) is the transcriptional master regulator of late B cell differentiation [7]. BLIMP1 is dispensable for the initiation of the ASC program but is necessary for the establishment of the terminally differentiated PC phenotype, mainly through suppression of its target genes [8–11]. The generation of PBs and long-lived PCs capable of secreting high-

affinity Igs of different classes provides the foundation for the establishment of protective humoral responses.

RIF1 (Rap1-Interacting Factor 1 Homolog / Replication Timing Regulatory Factor 1) is a multifunctional protein initially identified in budding yeast as a regulator of telomere length homeostasis [12]. In mammalian cells, RIF1 contributes to preserving genome stability during both DNA replication and repair. Under conditions of DNA replication stress, RIF1 protects nascent DNA at stalled forks from degradation, facilitating their timely restart [13–16]. During the repair of DNA double-strand breaks (DSBs), RIF1 participates in the 53BP1-Shieldin cascade that protects the broken DNA ends against nucleolytic resection, thus influencing the choice of which DSB repair pathway to engage [17–21]. In addition to these genome-protective functions, RIF1 plays a central role in the control of DNA replication timing programs in both yeast and higher eukaryotes [22–25]. Several studies have also implicated RIF1 in early mouse development [26–30]. This role appears independent from RIF1's various activities in DNA metabolism, and is mediated by its ability to modulate the transcriptional networks responsible for embryonic stem cell state stability and differentiation [26–30].

Isotype diversification by CSR occurs *via* a deletional recombination reaction at the Ig heavy chain (*Igh*) locus, which replaces the constant (C) region of the IgM/IgD basal isotype with one of the downstream C regions encoding for the different classes (IgG, IgE or IgA) [4]. The process is initiated by the B cell-specific enzyme Activation-Induced Deaminase (AID), whose activity at the *Igh* locus leads to the formation of DSBs that are obligate intermediates in the reaction [3]. These

64 programmed breaks need to be physiologically protected from extensive resection to
65 enable productive repair events and CSR [31]. Due to its ability to inhibit DSB end
66 processing, RIF1 is required for repair of *Igh* breaks, and hence for efficient Ig
67 isotype diversification [17–19]. In this study, we report a novel role for RIF1 in the
68 regulation of humoral immunity. We discovered that RIF1 expression is upregulated
69 in mature B cells following activation, where it binds cis-regulatory elements of genes
70 involved in B cell function and differentiation. RIF1 deficiency skews the
71 transcriptional profile of activated B cells towards PBs and PCs, and is associated
72 with an accelerated differentiation to ASCs both *ex* and *in vivo*. RIF1 directly binds
73 several BLIMP1 target genes and counteracts their premature repression. Thus,
74 RIF1 contributes an additional regulatory layer to the B cell differentiation program
75 that is essential to establish secreted antibody diversity.

## Results

### *Rif1* expression is regulated during B cell differentiation

Given RIF1's multiple roles during early development and in differentiated somatic cells [26,27,29,30,32,33], we asked whether RIF1 contributes functions beyond the regulation of DNA end processing and repair in B cells. To do so, we first monitored *Rif1* expression levels across B cell lineage developmental stages using the Immunological Genome Project (ImmGen) transcriptomics data [34]. *Rif1* expression varied considerably in the different B cell subtypes, with GC cells exhibiting the highest levels (Fig. 1a). In contrast, the expression of RIF1's up- and downstream partners in DNA end protection, 53BP1 and the Shieldin (MAD2L2-SHLD1-SHLD2-SHLD3) complex, respectively, did not show any major changes during B cell development and differentiation (Fig. 1a and S1a). In addition, *ex vivo* activation of isolated naïve B cells (Fig. 1b and S1b) resulted in upregulation of *Rif1* transcript levels, regardless of the stimulation condition (LPS and IL-4 (LI); LPS, BAFF and TGFβ (LBT); or LPS (L)) and resulting isotype switching (IgG1, IgG2b, or IgG3, respectively) (Fig. 1c). MAD2L2 was the only additional component of the 53BP1-RIF1-Shieldin axis to exhibit transcriptional induction after *ex vivo* stimulation (Fig. 1c and S1c). Finally, *Rif1* transcripts' upregulation was accompanied by an increase in the expression also at the protein level, which was readily detectable at 48 h after activation, sustained at 72 h and declining thereafter (Fig. 1d). We concluded that *Rif1* expression is induced following activation of mature B cells both *in* and *ex vivo*, and that this expression dynamics does not reflect a general behavior of DSB end protection factors.

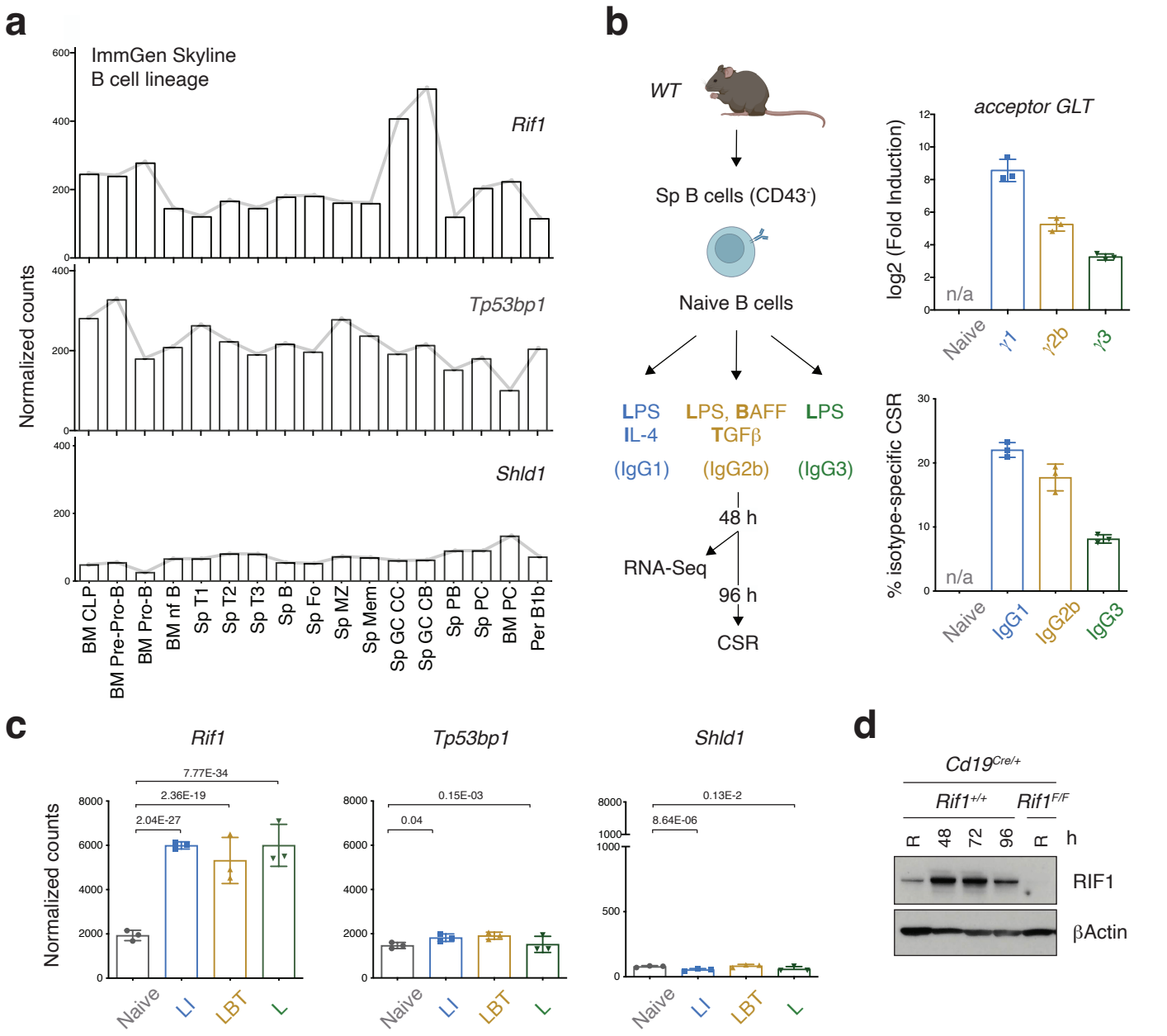


**Figure 1. *Rif1* expression is dynamically regulated during late B cell differentiation**. **a** Expression of *Rif1*, *Tp53bp1*, and *Shld1* genes across B cell lineage developmental stages as determined by the Immunological Genome Project (ImmGen) Skyline RNA-Seq analysis. BM: bone marrow; CLP: common lymphoid progenitor; nf: newly-formed; Sp: splenic; Fo: follicular; MZ: marginal zone; Mem: memory; GC: germinal center; CC: centrocytes; CB: centroblasts; PB: plasmablasts; PC: plasma cells; Per B1b: peritoneal B1b. **b** Left: Schematic representation of gene expression analysis in naïve B cells isolated from mouse spleens and stimulated *ex vivo* with LPS and IL-4 (LI cocktail), LPS, BAFF and TGFβ (LBT), or LPS only (L). Right: Levels of acceptor germline transcript (GLT) induced by LI-, LBT- or L-stimulation (expressed as fold increase over the naïve sample) and CSR efficiency to the corresponding isotype for each of the primary B cell cultures employed in the RNA-Seq analysis (n = 3 mice per stimulation condition). n/a: not applicable. **c** Expression of *Rif1*, *Tp53bp1*, and *Shld1* in naïve and LI/LBT/L-stimulated B cells. **d** Western blot analysis of *Cd19*$^{Cre/+}$ and *Rif1*$^{F/F}$*Cd19*$^{Cre/+}$ purified B lymphocytes at the indicated times after activation with LI. Data is representative of two independent genotype pairs. R: Resting. Expression values in panels **a**, **b** and **c** were normalized by DESeq2. The adjusted p-value of significant differences between samples in panel **c** is indicated.

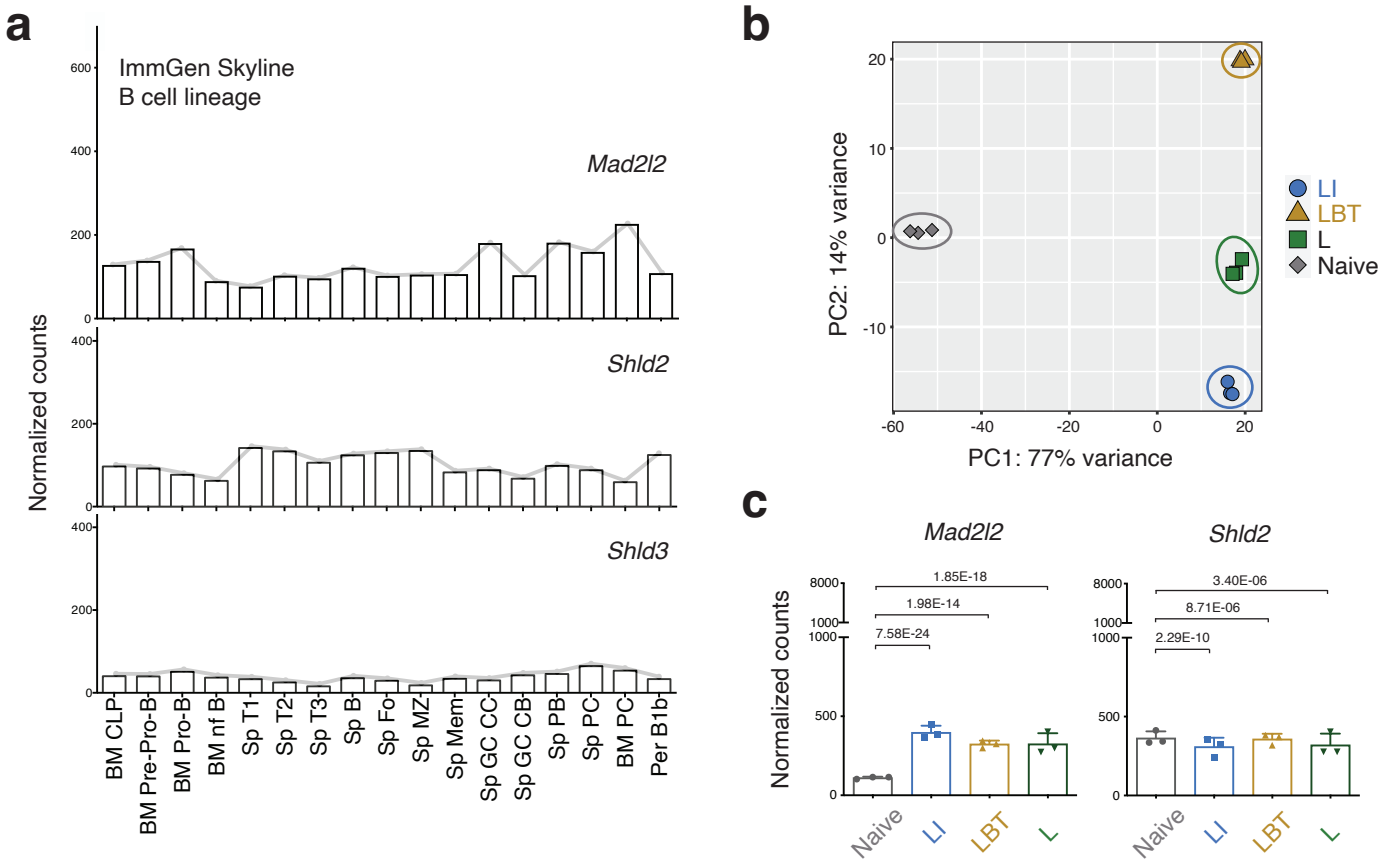


**Figure S1. Stimulation-dependent clustering of B cell transcriptomics profiles after *ex vivo* activation. a** Expression of *Mad2l2*, *Shld2* and *Shld3* genes across B cell lineage developmental stages as determined by the Immunological Genome Project (ImmGen) Skyline RNA-Seq analysis. BM: bone marrow; CLP: common lymphoid progenitor; nf: newly-formed; Sp: splenic; Fo: follicular; MZ: marginal zone; Mem: memory; GC: germinal center; CC: centrocytes; CB: centroblasts; PB: plasmablasts; PC: plasma cells; Per B1b: peritoneal B1b. **b** Principal component analysis for the RNA-Seq datasets of WT splenocytes before (naïve) and after 48 h stimulation with LPS and IL-4 (LI), LPS, BAFF and TGFβ (LBT), or LPS only (L). The RNA-Seq analysis was performed on three biological replicates/mice per condition. **c** Expression of *Mad2l2* and *Shld2* in naïve and LI/LBT/L-stimulated B cells. *Shld3* expression levels were below detection in all datasets. Expression values in panels **a** and **c** were normalized by DESeq2. The adjusted p-value of significant differences between samples in panel **c** is indicated. Related to Figure 1.

101 **RIF1 limits the *ex vivo* differentiation of activated B cells into PBs and PC-like**
102 **cells**
103 The specific upregulation of RIF1 expression in GC and *ex vivo* stimulated
104 splenocytes (Fig. 1) suggests that RIF1's functional repertoire in activated B cells
105 might extend beyond its established role in the regulation of DNA end processing. In
106 addition to SHM and CSR, activation of mature B cells triggers the late stages of B
107 cell development [5,6,35]. Therefore, we next investigated the potential involvement of
108 RIF1 during ASC generation.
109
110 Stimulation of naïve B cells with LPS and IL-4 induces their *ex vivo* differentiation into
111 PBs (evidenced by the surface expression of CD138). To assess the contribution of
112 RIF1 to this process, we employed B lymphocyte cultures from *Rif1*$^{F/F}$*Cd19*$^{Cre/+}$ mice
113 (Fig. 1d), which conditionally ablate *Rif1* expression at the immature B cell stage [18].
114 We found an over two-fold increase in the percentage of CD138$^{+}$ cells in
115 *Rif1*$^{F/F}$*Cd19*$^{Cre/+}$ samples compared to *Cd19*$^{Cre}$ (Fig. 2a), despite similar proliferation
116 rates between the two genotypes (Fig. 2b and [18]). Furthermore, whereas controls
117 exhibited a steep rise in PB formation mainly at the last cell division, RIF1-deficient
118 cultures showed higher and increasing levels of PBs from earlier division rounds
119 (Fig. 2b). The observed phenotype is not linked to RIF1's role in the regulation of
120 DNA end processing nor to the CSR defect associated to its ablation since B cell
121 cultures from mice lacking either a functional Shieldin complex (*Shld1*$^{-/-}$) or AID
122 (*Aicda*$^{-/-}$) differentiated to the same extent as controls (Fig. 2c).
123
124 Currently, no *in vitro* setting can fully recapitulate the complexity of PC differentiation
125 and function. However, the induced GC B (iGB) culture system ideated by Nojima *et*

126 *al.* mimics the T cell-dependent generation of GC B cells and enables the *in vitro*
127 manipulation of their fates into either memory- or long-lived PC-like cells [36] (Fig. 2d).
128 We took advantage of this system to assess the contribution of RIF1 to the terminal
129 differentiation of activated B cells *ex vivo*. At the GC-like phenotype stage (four days
130 stimulation with IL-4 on CD40L- and BAFF-expressing feeder cells), RIF1 deficiency
131 resulted in the expected severe defect in CSR (Fig. 2, d and e, and [17–19]). However,
132 and in agreement with their increased potential to differentiate into PBs (Fig. 2, a to
133 c), *Rif1*$^{F/F}$*Cd19*$^{Cre}$ B cells showed a near two-fold increase in the percentage of PC-
134 like cells after prolonged culturing in the presence of IL-21 (Fig. 2, d and f).
135
136 Altogether, these data indicate that RIF1 deficiency accelerates the *ex vivo*
137 differentiation of activated B cells to PBs and PC-like cells, and that this function is
138 independent from RIF1's role in DNA end protection and CSR.

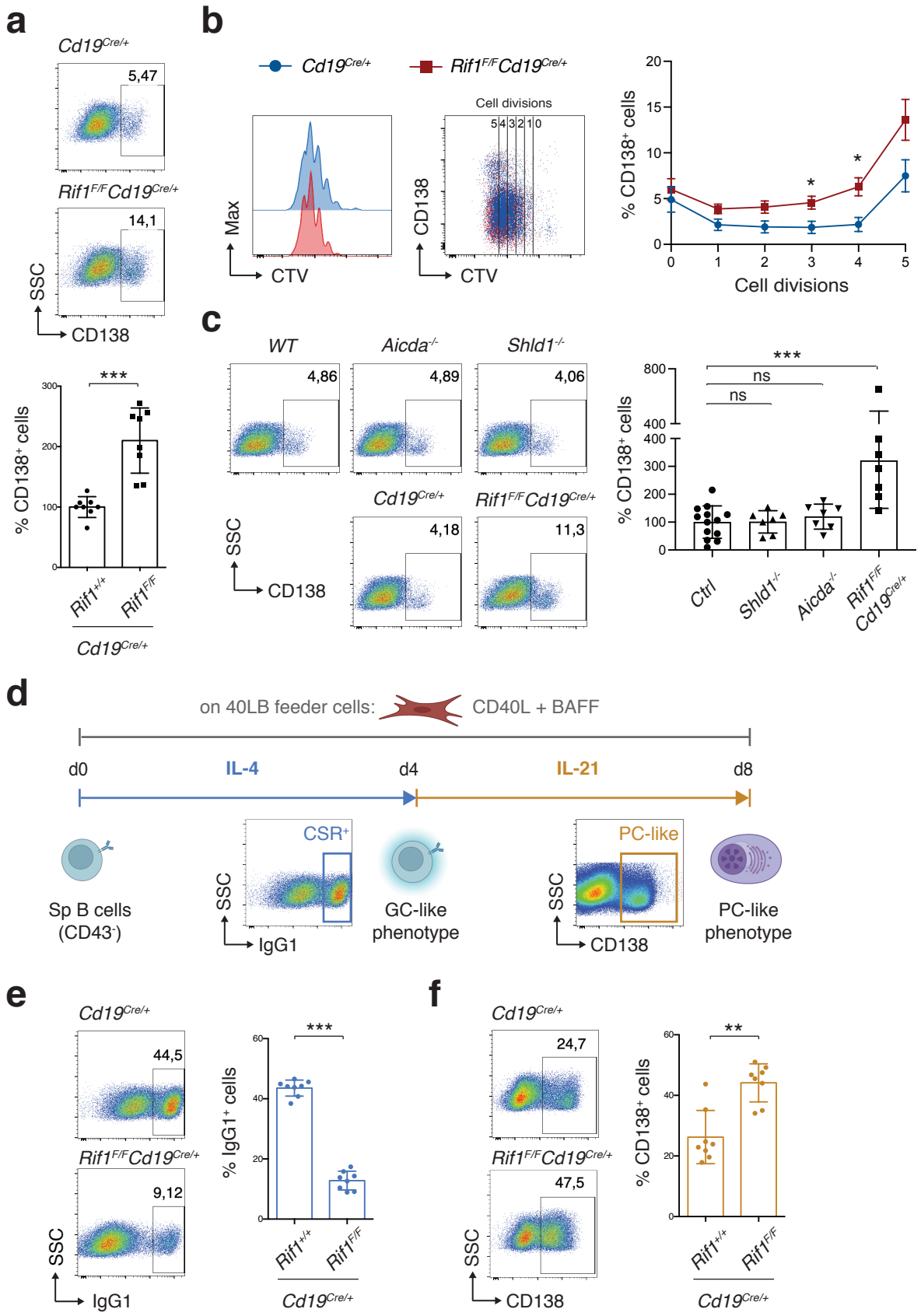
a
Cd19Cre/+
5,47
Rif1F/FCd19Cre/+
14,1
SSC
CD138
% CD138+ cells
***
Rif1+/+
Rif1F/F
Cd19Cre/+
b
Cd19Cre/+
Rif1F/FCd19Cre/+
Cell divisions
5 4 3 2 1 0
Max
CTV
CD138
% CD138+ cells
Cell divisions
c
WT
Aicda-/-
Shld1-/-
4,86
4,89
4,06
Cd19Cre/+
Rif1F/FCd19Cre/+
4,18
11,3
SSC
CD138
% CD138+ cells
***
ns
ns
Ctrl
Shld1-/-
Aicda-/-
Rif1F/F Cd19Cre/+
d
on 40LB feeder cells:
CD40L + BAFF
d0
IL-4
d4
IL-21
d8
Sp B cells
(CD43-)
CSR+
SSC
IgG1
GC-like
phenotype
PC-like
SSC
CD138
PC-like
phenotype
e
Cd19Cre/+
44,5
Rif1F/FCd19Cre/+
9,12
SSC
IgG1
% IgG1+ cells
***
Rif1+/+
Rif1F/F
Cd19Cre/+
f
Cd19Cre/+
24,7
Rif1F/FCd19Cre/+
47,5
SSC
CD138
% CD138+ cells
**
Rif1+/+
Rif1F/F
Cd19Cre/+

**Figure 2. RIF1 limits the *ex vivo* differentiation of activated B cells to PBs and PC-like cells independently from its role in DNA end protection and CSR. a** Top: Representative flow cytometry plots measuring percentage of plasmablasts (CD138+) in purified splenic B cell cultures of the indicated genotypes 96 h after activation with LPS and IL-4 (LI). Bottom: Summary graph for five independent experiments (n = eight mice per genotype), with % of CD138+ cells within each experiment normalized to the average of control mice ($Cd19^{Cre/+}$), which was set to 100%. **b** Left: Representative flow cytometry plots measuring proliferation by CellTrace Violet (CTV) dilution and percentage of CD138+ cells per cell division in primary cultures of $Cd19^{Cre/+}$ and $Rif1^{F/F}Cd19^{Cre/+}$ B lymphocytes stimulated with LI for 96 h. Right: Summary graph for three independent experiments (n = 6 mice per genotype). **c** Left: Representative flow cytometry plots measuring percentage of CD138+ cells in purified B cell cultures of the indicated genotypes 96 h after activation with LI. Right: Summary graph for four independent experiments (n = seven mice per genotype) with % of CD138+ cells within each experiment normalized to the average of control mice (*WT* and $Cd19^{Cre/+}$: *Ctrl*), which was set to 100%. **d** Schematic representation of the iGB (induced germinal center (GC) phenotype B) cell culture system for the *ex vivo* differentiation of splenic naïve B cells to GC- and plasma cell-like cells. CD40L: CD40 ligand; d: day; Sp: splenic; CSR+: class switched cells; PC: plasma cell. **e**-**f** Left: Representative flow cytometry plots measuring CSR to IgG1 (**e**) and percentage of plasmablasts (CD138+) (**f**) in purified B cell cultures of the indicated genotypes at day 4 (**e**) and 8 (**f**), respectively, of the iGB cell culture system shown in panel **d**. Right: Summary graphs for five independent experiments (n = eight mice per genotype). Significance in panels **a**, **b**, **c**, **e** and **f** was calculated with the Mann–Whitney U test, with error bars representing SD in panels **a**, **c**, **e** and **f**, and SEM in panel **b**. Only significant differences between groups were indicated in panel **b**. ns: not significant; * = $p \leq 0.05$; ** = $p \leq 0.01$; *** = $p \leq 0.001$.

139 **RIF1 deficiency does not affect GC B cell dynamics**

140 We next asked whether RIF1 is able to modulate late B cell differentiation also *in*
141 *vivo*. To this end, we first assessed the consequences of RIF1 ablation on GC
142 physiology by comparing GC B cell dynamics in Peyer's patches (PPs) of *Cd19*$^{Cre/+}$
143 and *Rif1*$^{F/F}$*Cd19*$^{Cre/+}$ mice. GCs are anatomically separated into the dark zone (DZ)
144 and light zone (LZ) [5,6], and cycling of positively selected GC B cells between LZ and
145 DZ ensures further affinity maturation and clonal expansion [5,6]. PPs are specialized
146 secondary lymphoid structures that line the wall of the small intestine and are crucial
147 for mucosal IgA antibody responses [37]. PPs allow for the assessment of chronic GC
148 activity in response to a variety of food- and microbiome-derived antigens.

149

150 Control and *Rif1*$^{F/F}$*Cd19*$^{Cre/+}$ mice showed no significant difference in the percentage
151 of PP GC B cells nor in their distribution in the LZ *versus* DZ (Fig. 3, a and b). In
152 contrast, mice knock-out for AID exhibited the expected massive increase in GC B
153 cells and a cellular distribution heavily skewed towards the LZ (Fig. 3b and [38–40]).
154 Interestingly, despite the severe CSR defect caused by RIF1 deficiency [17–19,31], PPs
155 of *Rif1*$^{F/F}$*Cd19*$^{Cre/+}$ mice displayed near-physiological levels of IgA$^{+}$ GC B cells (Fig.
156 3, a and b), thus indicating that the few cells that successfully class-switch are
157 actively selected forward in this context. We concluded that under conditions of
158 chronic stimulation, RIF1 is dispensable for GC B cell formation, selection and
159 proper DZ/LZ compartmentalization.

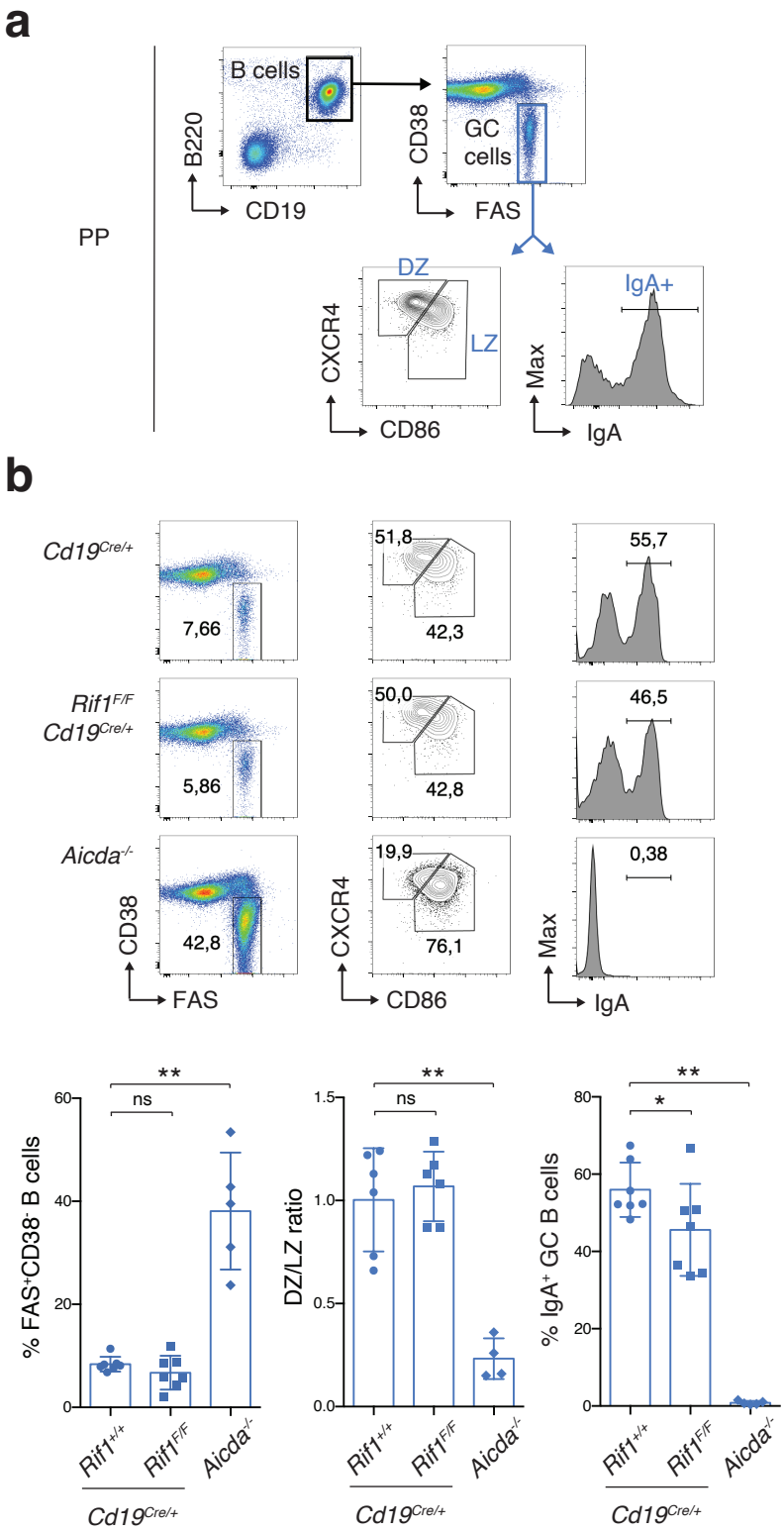


**Figure 3. RIF1 deficiency does not affect GC B cell dynamics. a** Gating strategy for Germinal Center (GC) analysis in Payer's Patches (PPs). DZ: dark zone; LZ: light zone. **b** Top: Representative flow cytometry plots measuring percentage of GC B cells, DZ/LZ and IgA+ fraction of GC B cells in PPs of *Cd19*$^{Cre/+}$, *Rif1*$^{F/F}$*Cd19*$^{Cre/+}$ *and Aicda*$^{-/-}$ mice. Bottom: Summary graphs for at least four mice per genotype in at least three independent experiments. Significance in panel **b** was calculated with the Mann–Whitney U test and error bars represent SD. ns: not significant; * = $p \leq 0.05$; ** = $p \leq 0.01$.

160 **RIF1 curtails plasma cell formation following immunization**

161 Next, we analyzed the GC and PC compartment of control and *Rif1*$^{F/F}$*Cd19*$^{Cre/+}$ mice
162 immunized with the T-cell-dependent antigen 4-Hydroxy-3-nitrophenylacetyl hapten
163 conjugated to Chicken Gamma Globulin (NP-CGG) (Fig. 4a). In contrast to chronic
164 stimulation, NP-CGG immunization elicited a reduced number of GC B cells in the
165 absence of RIF1 (Fig. S2, a and b). This phenotype is likely due to higher levels of
166 apoptosis induced by unrepaired DSBs, as we have previously shown [18], or DNA
167 end resection-dependent BCR loss [41]. As expected for an acute immune response
168 context, the levels of class-switched IgG1$^{+}$ GC B cells
169 (CD19$^{+}$B220$^{+}$FAS$^{high}$CD38$^{low}$IgG1$^{+}$) were decreased in *Rif1*$^{F/F}$*Cd19*$^{Cre}$ mice (Fig. S2,
170 a and b).

171

172 Despite the reduced number of GC B cells, *Rif1*$^{F/F}$*Cd19*$^{Cre}$ mice displayed a
173 consistent increase in the total pool of terminally differentiated PCs
174 (TACI$^{+}$CD138$^{+}$AA4.1$^{+}$MHCII$^{-}$) compared to controls in both spleen and bone marrow
175 at earlier time points post-immunization (day 7 and 14 in the spleen and day 14 in
176 the bone marrow) (Fig. 4b). The higher proportion of PCs observed at day 7 in the
177 spleen occurs on the background of a reduced ASC pool (Fig. 4b), which suggests
178 that terminal B cell differentiation is accelerated in the absence of RIF1 also *in vivo*.
179 The phenotype was no longer observed in either compartment at later time points
180 (day 28, Fig. 4b) nor in unimmunized mice (Fig. S3 and [17]). However, functional
181 assessment of NP-specific PCs by ELISpot analysis showed a sustained trend
182 towards higher levels of ASCs in the bone marrow of *Rif1*$^{F/F}$*Cd19*$^{Cre/+}$ mice compared
183 to controls, which was particularly pronounced at later time points after immunization

184 (Fig. 4c). This latter observation is in agreement with the ability of terminally
185 differentiated PCs to home to the bone marrow.
186
187 These findings indicate that RIF1 deletion removes a physiological restraint imposed
188 over the terminal differentiation of mature B cells *in vivo*, which, though concealed
189 under steady-state conditions, is readily detectable at the systemic level upon
190 immunization. Furthermore, taking into consideration also the *ex vivo* recapitulation
191 of the increased ASC phenotype (Fig. 2) and unaffected GC B cell dynamics (Fig. 3),
192 we concluded that RIF1's ability to delay terminal B cell differentiation *in vivo* reflects
193 a cell-intrinsic property independent from the GC reaction.

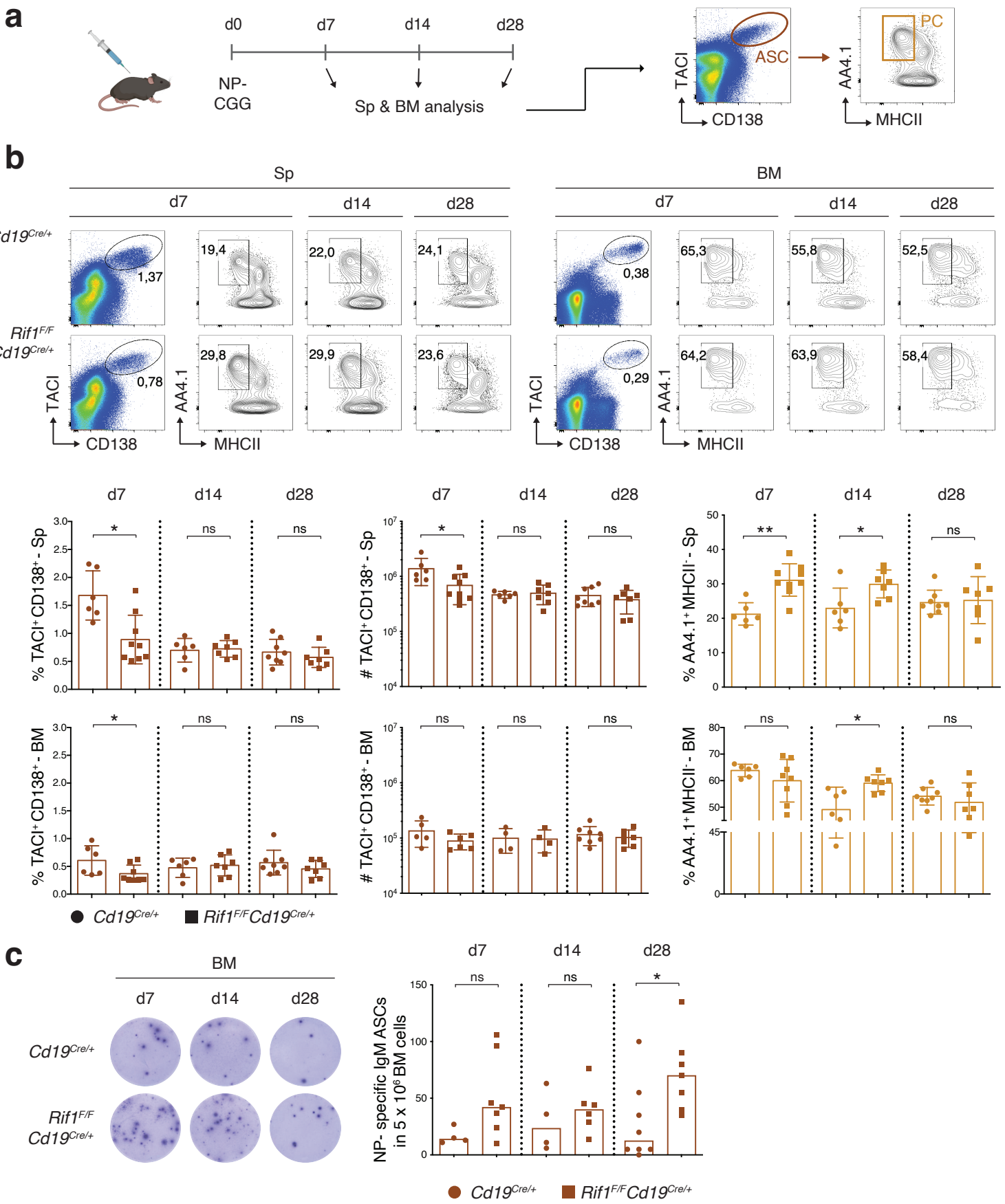
a
d0
d7
d14
d28
NP-CGG
Sp & BM analysis
TACI
CD138
ASC
AA4.1
MHCII
PC
b
Sp
BM
d7
d14
d28
Cd19Cre/+
Rif1F/F Cd19Cre/+
1,37
19,4
22,0
24,1
0,38
65,3
55,8
52,5
0,78
29,8
29,9
23,6
0,29
64,2
63,9
58,4
% TACI+CD138+ - Sp
# TACI+CD138+ - Sp
% AA4.1+MHCII- - Sp
% TACI+CD138+ - BM
# TACI+CD138+ - BM
% AA4.1+MHCII- - BM
ns
*
**
Cd19Cre/+
Rif1F/F Cd19Cre/+
c
BM
NP- specific IgM ASCs in 5 x 10^6 BM cells

**Figure 4. Ablation of RIF1 enhances plasma cell formation after immunization. a** Schematic representation of the NP-CGG immunization protocol and gating strategy employed for the phenotypic analysis of the plasma cell compartment. d: day; NP-CGG: 4-hydroxy-3-nitrophenylacetyl hapten conjugated to Chicken Gamma Globulin; Sp: spleen; BM: bone marrow; ASC: antibody secreting cell; PC: plasma cell. **b** Top: Representative flow cytometry plots measuring percentage of antibody secreting cells and plasma cells in spleens and bone marrows of *Cd19*$^{Cre/+}$ and *Rif1*$^{F/F}$*Cd19*$^{Cre/+}$ mice at the indicated days after immunization. Bottom: Summary graphs for at least six mice per genotype and time point in at least 3 independent experiments. **c** Left: Representative ELISpot analysis of NP-specific IgM ASCs in the BM at the indicated times after immunization. Right: Summary graph showing the number of NP-specific IgM ASCs per 5 x $10^6$ BM cells for at least four mice per genotype and time point. Significance in panels **b** and **c** was calculated with the Mann–Whitney U test. ns: not significant; * = $p \leq 0.05$; ** = $p \leq 0.01$. Error bars in panel **b** represent SD whereas the graph in panel **c** show the median of each dataset.

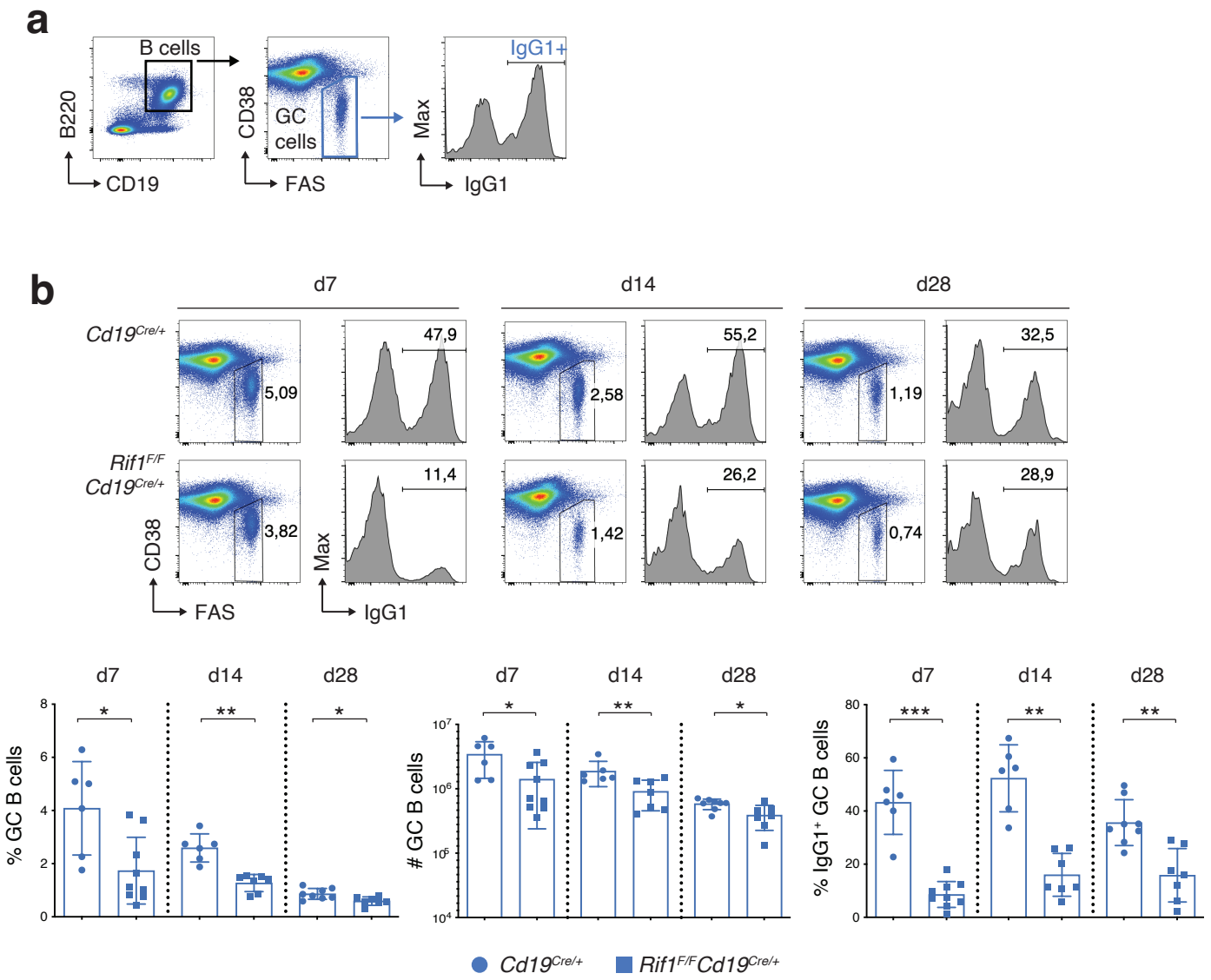


**Figure S2. RIF1 deficiency results in a reduced number of class-switched GC B cells upon immunization. a** Gating strategy for Germinal Center (GC) analysis. **b** Top: Representative flow cytometry plots measuring the percentage of GC cells and IgG1-class switched GC cells in spleens of *Cd19*$^{Cre/+}$ and *Rif1*$^{F/F}$*Cd19*$^{Cre/+}$ mice at the indicated days after immunization. Bottom: Summary graphs for at least six mice per genotype and time point in at least three independent experiments. Significance in panel **b** was calculated with the Mann–Whitney U test and error bars represent SD. * = $p \leq 0.05$; ** = $p \leq 0.01$; *** = $p \leq 0.001$. Related to Figure 4.

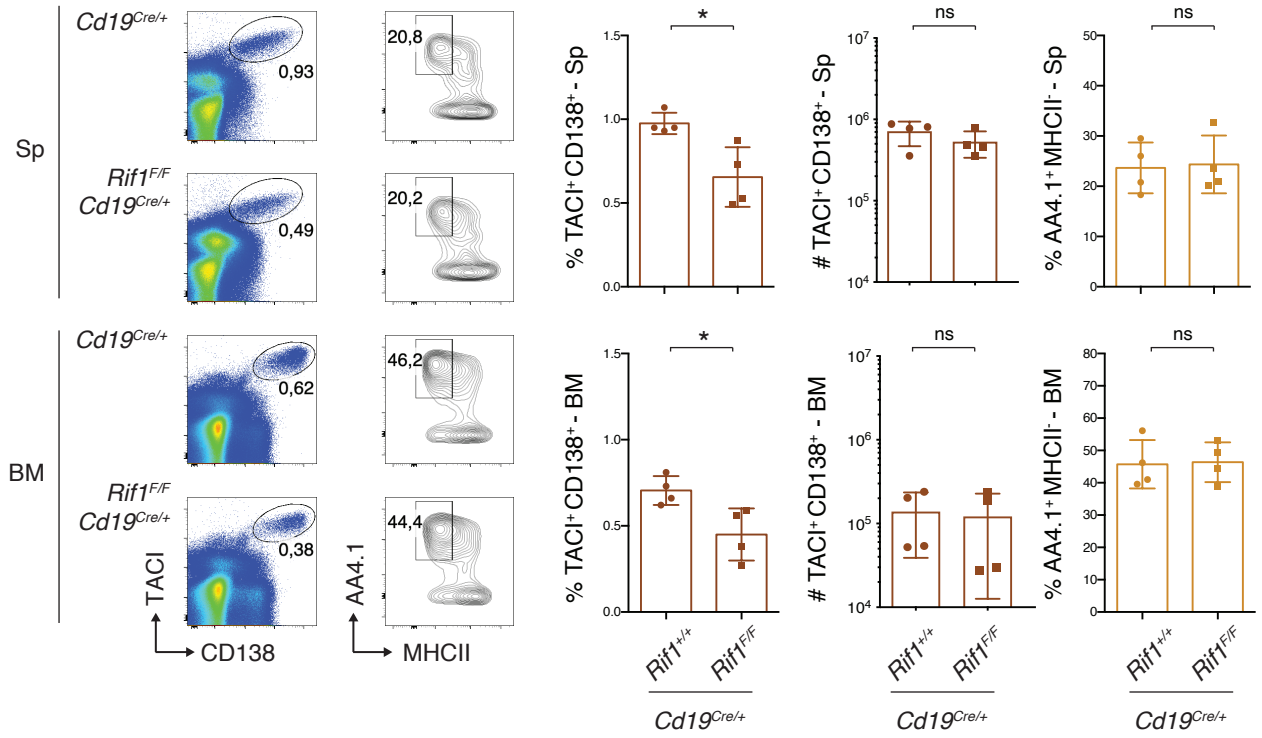


**Figure S3. RIF1 ablation does not result in detectable changes of the plasma cell compartment in steady state condition.** Left: Representative flow cytometry plots measuring percentage of antibody secreting cells and plasma cells in spleens and bone marrows of unimmunized mice of the indicated genotypes. The same gating strategy as in Figure 4a was employed. Sp: spleen; BM: bone marrow. Right: Summary graphs for four mice per genotype. Significance was calculated with the Mann–Whitney U test, and error bars represent SD. ns: not significant; * = $p \leq 0.05$. Related to Figure 4.

194 **RIF1 deficiency skews the transcriptional profile of activated B cells towards**
195 **ASCs**
196 RIF1 has been implicated in the modulation of transcriptional programs responsible
197 for embryonic stem cell differentiation [27,30,33,42]. Therefore, we asked whether the
198 increased potential for terminal B cell differentiation in the absence of RIF1 reflects a
199 transcriptional role in the modulation of B cell identity.
200
201 Activation of isolated splenic B cells with specific stimuli recapitulates several
202 features of terminal B cell differentiation (Fig. 2 and [10,43]). Hence, we monitored the
203 consequences of RIF1 deficiency on the mature B cell transcriptome after *ex vivo*
204 activation with LPS and IL-4. Comparative assessment of the transcriptional profiles
205 of *Cd19*$^{Cre/+}$ and *Rif1*$^{F/F}$*Cd19*$^{Cre/+}$ B cells identified only a limited number of
206 considerably deregulated genes in the absence of RIF1 (N° genes with log2 FC < -1
207 and > 1 = 0, 105, and 47 at 48, 72, and 96 h, respectively) (Fig. 5, a and b, S4, a and
208 b, and Table S1). Furthermore, the expression of the mature B cell identity
209 transcriptional regulators (*Pax5*, *Ebf1*, *Foxo1,* and *Bach2*) was not affected (Fig. 5c).
210 However, when we assessed the status of the key factors driving the ASC program
211 (*Prdm1*, *Irf4*, and *Xbp1*), we found a near 2-fold increase in *Prdm1* transcript levels
212 at 96 h after activation (Fig. 5, b and c). Since the *Prdm1*-encoded transcription
213 factor BLIMP1 is required for the differentiation of pre-PBs into PBs and PCs [8,10], we
214 cross-referenced the list of differentially expressed genes (DEG, adjusted p-value <
215 0.05) from *Rif1*$^{F/F}$*Cd19*$^{Cre/+}$ activated B cells (Table S1) with the PB and PC
216 signatures [10] (see Data analysis section of Methods). We observed a significant
217 overlap between DEGs and the corresponding up-/down-regulated gene set in the
218 ASC signatures, with the tendency being more pronounced for the down-regulated

219 datasets (Fig. 5d, S4c and Table S2). We concluded that RIF1 deficiency in
220 activated B cells results in a deregulated expression profile enriched in genes
221 normally expressed in terminally differentiated B cells.

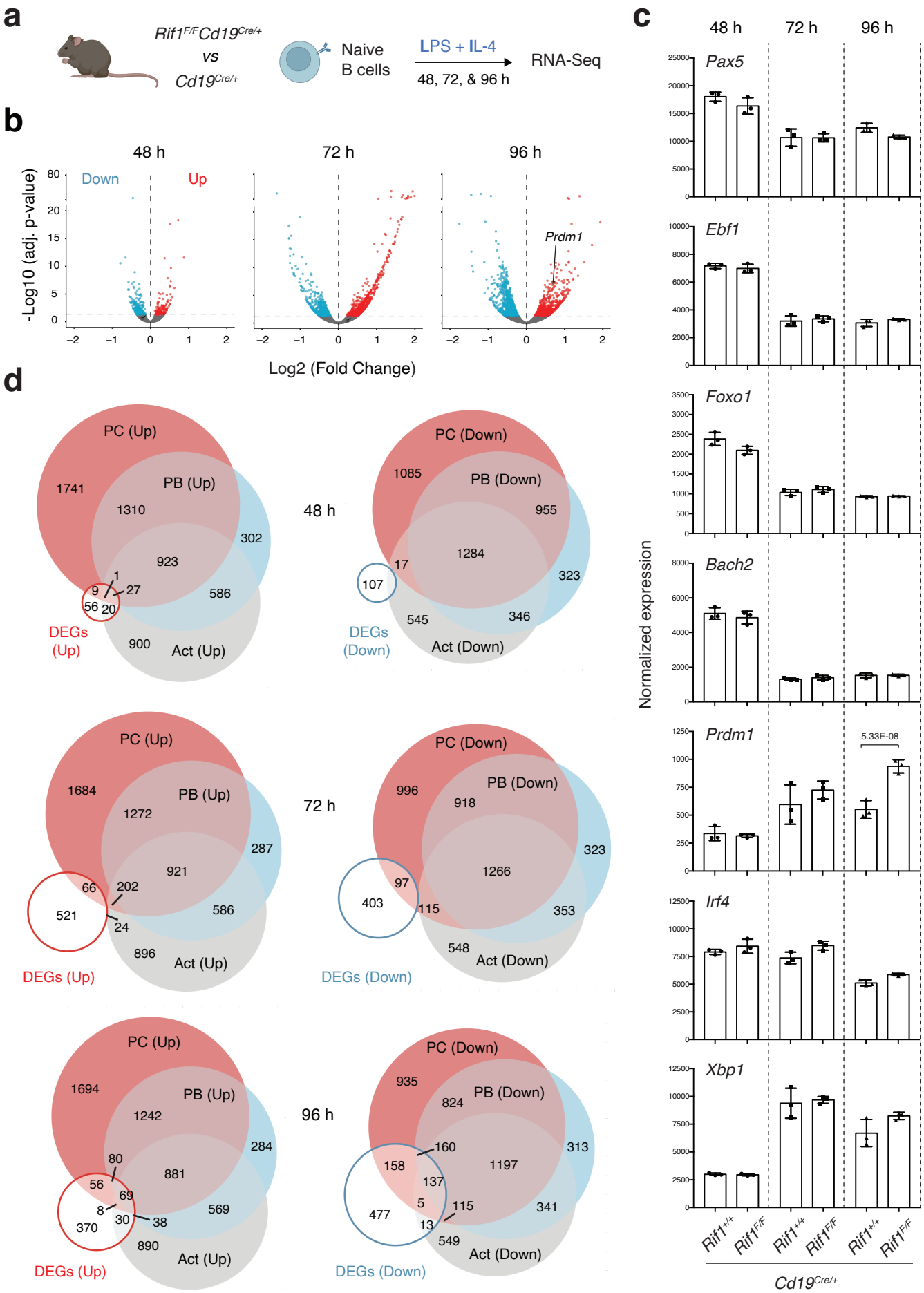
a
Rif1F/F Cd19Cre/+
vs
Cd19Cre/+
Naive
B cells
LPS + IL-4
48, 72, & 96 h
RNA-Seq
b
48 h
72 h
96 h
Down
Up
Prdm1
-Log10 (adj. p-value)
Log2 (Fold Change)
c
48 h
72 h
96 h
Pax5
Ebf1
Foxo1
Bach2
Prdm1
Irf4
Xbp1
5.33E-08
Normalized expression
Rif1+/+
Rif1F/F
Cd19Cre/+
d
PC (Up)
PB (Up)
Act (Up)
DEGs (Up)
PC (Down)
PB (Down)
Act (Down)
DEGs (Down)
48 h
72 h
96 h

**Figure 5. RIF1 deficiency skews the transcriptional profile of activated B cells towards ASCs**. **a** Schematic representation of gene expression analysis in naïve B cells isolated from *Cd19*$^{Cre/+}$ and *Rif1*$^{F/F}$*Cd19*$^{Cre/+}$ mouse spleens and stimulated *ex vivo* with LI for 48, 72, and 96 h. For the 48 h time point, the analysis was performed also on LBT-stimulated cultures. **b** Volcano plots displaying differentially expressed genes between control and RIF1-deficient splenocytes. The blue and red dots represent transcripts down- and up-regulated (adjusted p-value <= 0.05, blue horizontal dotted line), respectively, in *Rif1*$^{F/F}$*Cd19*$^{Cre/+}$ cells. **c** Expression of *Pax5, Ebf1, Foxo1, Bach2, Irf4, Xbp1,* and *Prdm1* as determined by the RNA-Seq. Values were normalized by DESeq2 and the adjusted p-value of the only significant difference between samples is indicated. **d** Venn diagrams depicting the overlaps between genes up- (left) and down- (right) regulated in RIF1-deficient splenocytes at the indicated times post-activation and the corresponding up-and down-regulated (over naïve B cells) categories in the activated (Act) B cell, PB, and PC transcriptional signatures (Minnich et al. 2016).

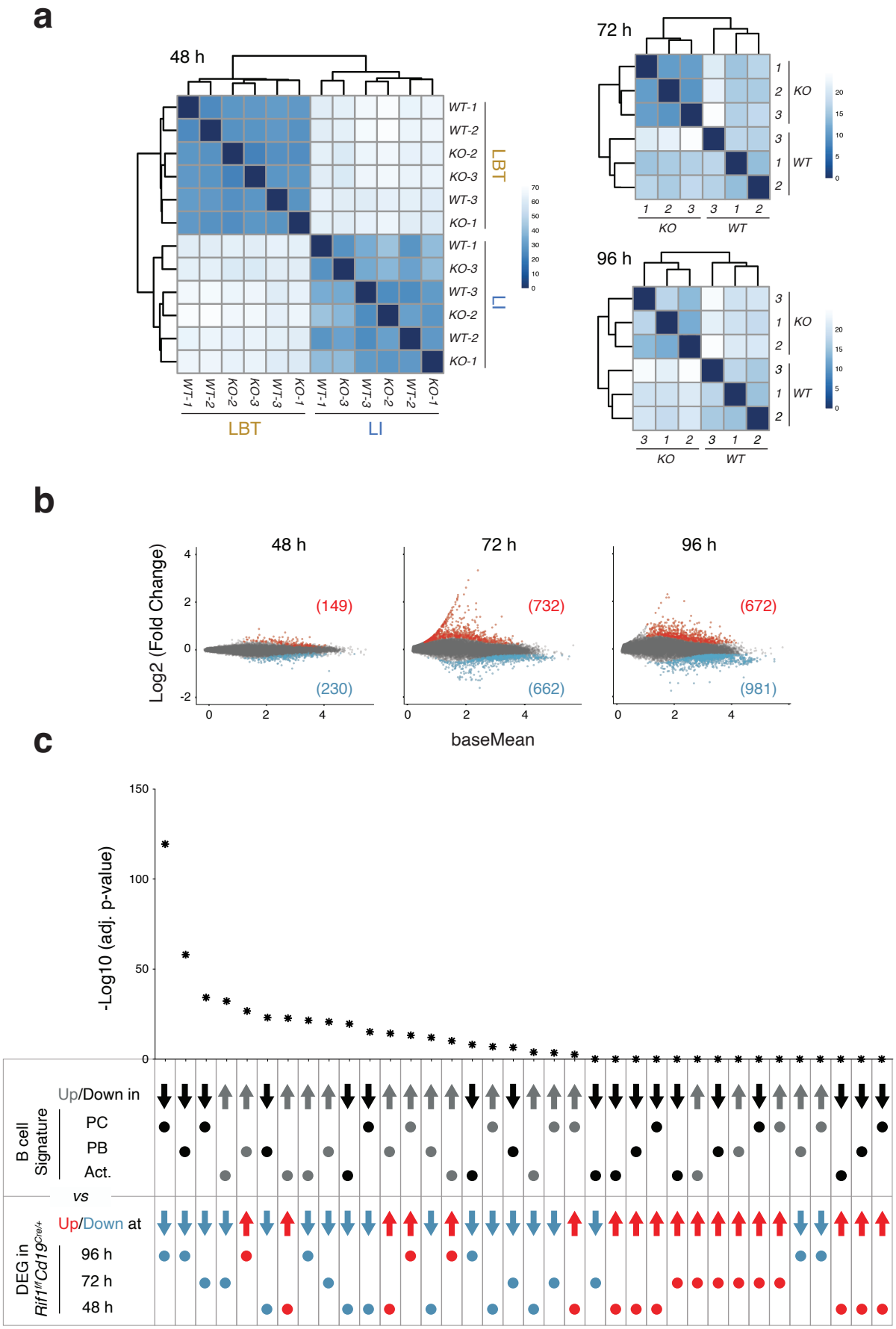
a
48 h
WT-1
WT-2
KO-2
KO-3
WT-3
KO-1
LBT
LI
72 h
96 h
KO
WT
b
48 h
72 h
96 h
Log2 (Fold Change)
(149)
(230)
(732)
(662)
(672)
(981)
baseMean
c
-Log10 (adj. p-value)
Up/Down in
B cell Signature
PC
PB
Act.
vs
Up/Down at
DEG in Rif1f/fCd19Cre/+
96 h
72 h
48 h

**Figure S4. RIF1 deficiency alters the transcriptional landscape of activated B cells. a-b** Dendrograms (**a**) and scatterplots (**b**) for the RNA-Seq datasets generated according to the experimental scheme depicted in Fig. 5a. For the 48 h time point, the analysis was performed on both LI- and LBT-stimulated cultures. Data summarizes results from three mice per genotype per stimulation condition. In the scatterplots, genes with an adjusted p-value <= 0.05 that are up- or down-regulated in *Rif1*$^{F/F}$*Cd19*$^{Cre/+}$ cells are highlighted in red or blue, respectively, and the number of DEGs per category is included in parenthesis. **c** Statistical significance of pairwise comparisons between the indicated gene lists *via* hypergeometric analysis. Related to Figure 5.

222 **RIF1 binds genes involved in the modulation of adaptive immune responses**

223 To uncover the molecular mechanism underlying RIF1 ability to maintain the
224 transcriptional identity of mature B cells after activation, we monitored the genome-
225 wide occupancy of RIF1 in activated B cells from *Rif1*$^{FH/FH}$ mice under the same
226 stimulation conditions employed for the *ex vivo* transcriptional analyses (Fig. 6a, [25]).
227 *Rif1*$^{FH/FH}$ splenocytes express physiological levels of a knock-in 1×Flag-
228 2×Hemagglutinin-tagged version of RIF1 (RIF1$^{FH}$, [44]) that supports its roles in mouse
229 embryonic fibroblasts, embryonic stem cells, and B cells [18,23,44]. We found that the
230 vast majority of RIF1 peaks colocalized with promoters (56,4 %) and distal intergenic
231 regions (25,4 %) (Fig. 6b). We next performed a functional enrichment analysis *via*
232 Genomic Regions Enrichment of Annotations Tool (GREAT) [45] to assess the
233 functional significance of both proximal- and distal-to-gene RIF1-binding events. We
234 identified several categories of genes associated with the regulation of lymphocyte
235 activation, function, and differentiation (Fig. 6c and Table S3). Altogether, these
236 findings indicate that in activated B cells, RIF1 associates with cis-regulatory
237 elements of genes involved in the modulation of the adaptive immune response.

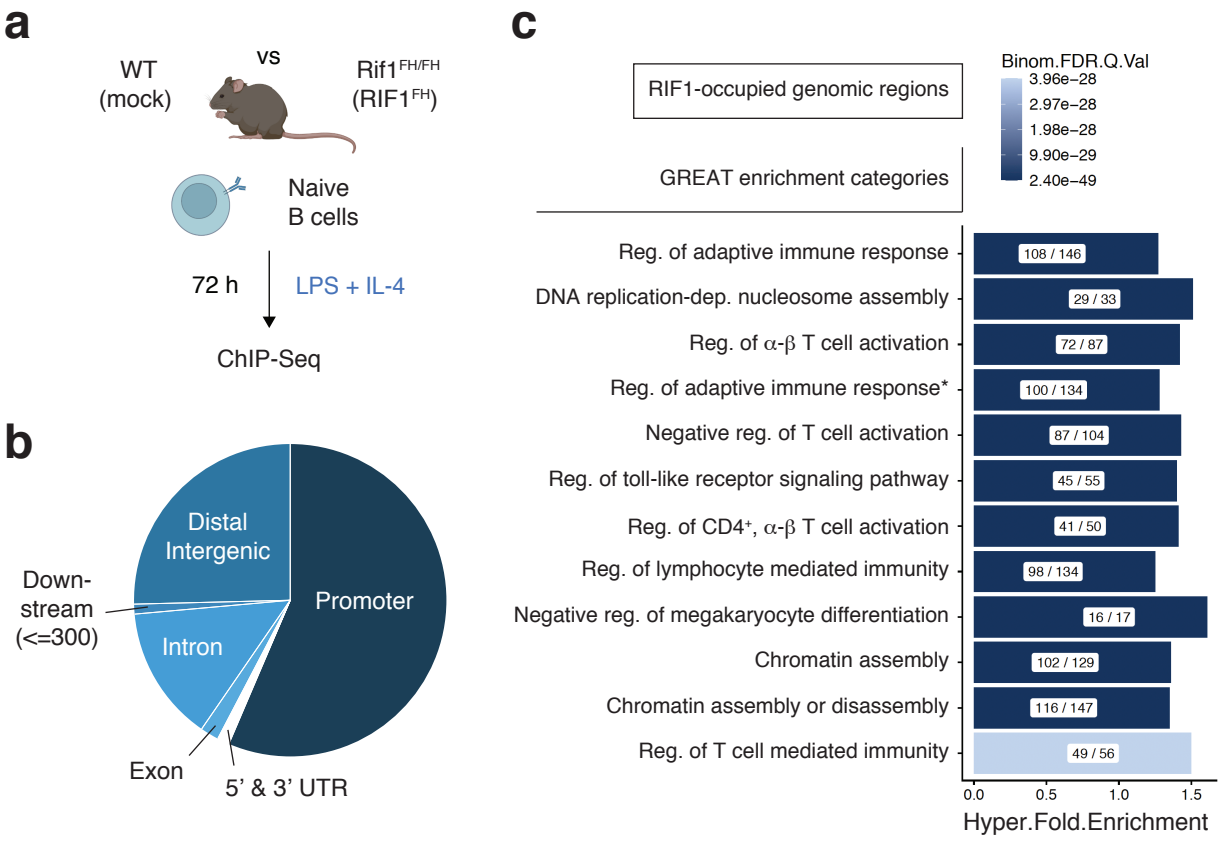


**Figure 6. RIF1-occupied genomic regions in activated B cells comprise genes involved in lymphocyte activation and differentiation. a** Schematic representation of the ChIP-Seq analysis in mature B cells isolated from spleens of *Rif1*$^{FH/FH}$ mice and stimulated *ex vivo* with LPS and IL-4 (LI). **b** Genomic distribution of RIF1-occupied annotated regions. **c** Gene ontology enrichment analysis as determined by GREAT for the genomic regions bound by RIF in LI-stimulated B cells. The complete name of the category marked with " * " is "Regulation of adaptive immune response based on somatic recombination of immune receptors built from immunoglobulin superfamily domain". The X / Y ratio within each bar indicates the number of genes occupied by RIF1 (X) out of the total number of genes in the category (Y). Reg: regulation; FDR: false discovery rate.

238 **RIF1 counteracts the premature repression of BLIMP1 target genes**

239 To further dissect how RIF1 modulates the transcriptional program driving B cell
240 differentiation into ASCs, we next explored the relationship between RIF1 and
241 BLIMP1, the key transcriptional regulator of terminal B cell differentiation [10,25]. To this
242 end, we first assessed the two factors' relative genome occupancy by comparing
243 RIF1 peaks (Fig. 6b) with BLIMP1-bound regions in activated B cells (see Methods).
244 We found that 1300 genomic regions (corresponding to 1144 genes) were co-
245 occupied by the two factors (Fig. 7a) and they primarily comprised active genes (Fig.
246 7b).

247

248 Since gene binding is not indicative *per se* of regulatory activity, we next investigated
249 the link between gene occupancy and transcriptional output. To this end, we first
250 asked whether RIF1 deficiency affects the transcriptional status of BLIMP1 targets,
251 which are defined as BLIMP1-occupied genes that are either up- (repressed, 121
252 targets) or down- (activated, 93 targets) regulated following its ablation [10]. We found
253 that several BLIMP1-activated genes were significantly up-regulated in
254 *Rif1*$^{F/F}$*Cd19*$^{Cre/+}$ cells at 96 h post-activation (Fig. 7c), which is line with the increased
255 differentiation potential of these cultures (Fig. 5). More interestingly, BLIMP1-
256 repressed targets were tendentially downregulated in the absence of RIF1, with the
257 phenotype being evident from earlier time points after activation (Fig. 7c).

258

259 Next, we assessed RIF1 occupancy at BLIMP1 targets that are differentially
260 expressed in the absence of RIF1. We found that a considerable portion of BLIMP1
261 repressed targets that are prematurely downregulated in the absence of RIF1 was
262 also occupied by RIF1 in wild-type (*Rif1*$^{FH/FH}$) cells at each time point post-activation,

263 which is indicative of a direct RIF1 modulatory function on these genes (Fig. 7, d and
264 e, and Table S4). This subset of targets comprises several genes whose repression
265 has already been phenotypically and/or functionally linked to late B cell
266 differentiation, including *Nedd4*, *Cd22*, *Ccr7*, *Btg1*, *Sell*, *B3gnt5*, *Bank1*, *Notch2*, and
267 *Id3* (Fig. 7d and Table S4) [10,11,46–55]. In contrast, the corresponding overlap for the
268 upregulated BLIMP1 target genes was much more limited and only evident at later
269 time points (Fig. 7d and Table S4). Altogether, these findings indicate that RIF1
270 supports the expression of several genes that are physiologically down-regulated by
271 BLIMP1 as part of the transcriptional program promoting B cell differentiation into
272 ASCs.

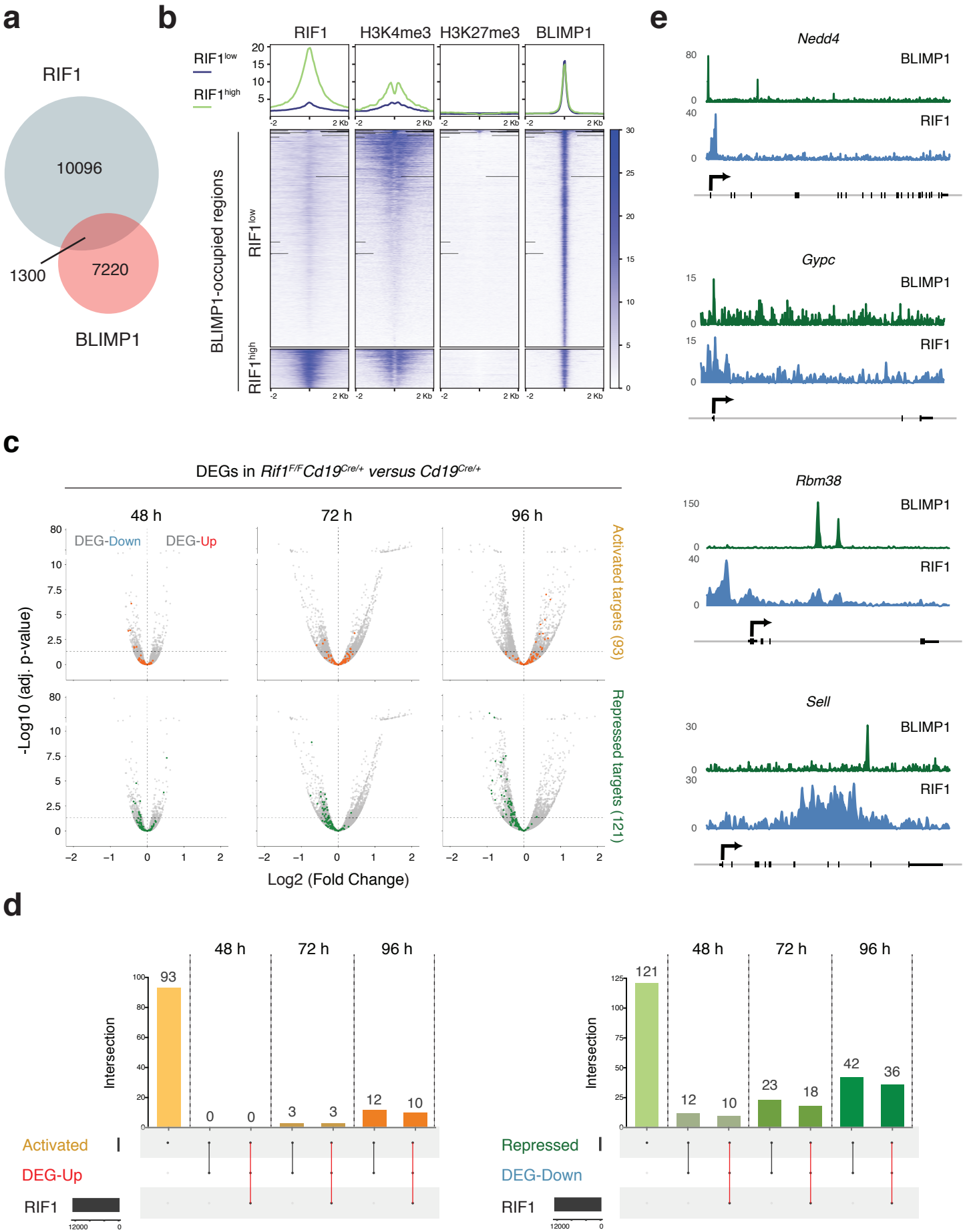
a
RIF1
10096
1300
7220
BLIMP1
b
RIF1
H3K4me3
H3K27me3
BLIMP1
RIF1low
RIF1high
BLIMP1-occupied regions
-2
2 Kb
e
Nedd4
BLIMP1
RIF1
Gypc
Rbm38
Sell
c
DEGs in Rif1F/FCd19Cre/+ versus Cd19Cre/+
48 h
72 h
96 h
DEG-Down
DEG-Up
Activated targets (93)
Repressed targets (121)
-Log10 (adj. p-value)
Log2 (Fold Change)
d
Intersection
93
0
0
3
3
12
10
Activated
DEG-Up
RIF1
121
12
10
23
18
42
36
Repressed
DEG-Down

**Figure 7. RIF1 counteracts the premature repression of BLIMP1 target genes. a** Venn diagram depicting the overlap between RIF1- and BLIMP1-bound genomic regions in activated B cells. **b** Line plots (top) and heatmaps (bottom) depicting the comparative genome distribution of RIF1, H3K4me3, and H3K27me3 in reference to BLIMP1-occupied regions. The line plots illustrate the mean normalized signal distribution of the indicated proteins, whereas the heatmaps visualize their signal strength at each identified peak. The x-axis in both graph types represents the genomic region relative to the peak center. **c** Volcano plots displaying BLIMP1-activated (in orange, top) and -repressed (in green, bottom) target genes among the transcripts (in grey both up- and down-regulated) identified in the *Cd19*$^{Cre/+}$ *versus* *Rif1*$^{F/F}$*Cd19*$^{Cre/+}$ transcriptome analysis shown in Fig. 5. The horizontal dotted line in the plots denotes the adjusted p-value of 0.05. **d** UpSet plots depicting the intersection between activated BLIMP1 targets (Activated), genes differentially upregulated in *Rif1*$^{F/F}$*Cd19*$^{Cre/+}$ B cells (DEG-Up) and RIF1-occupied regions (top), and between repressed BLIMP1 targets (Repressed), genes differentially downregulated in *Rif1*$^{F/F}$*Cd19*$^{Cre/+}$ B cells (DEG-Down) and RIF1-occupied regions (bottom). The dot matrixes at the bottom of each graph show the intersection relationships among the data sets, with the number of common elements in the intersecting sets indicated above each bar. The red lines in the matrixes highlight the group of genes occupied and regulated by both BLIMP1 and RIF1. **e** ChIP-seq tracks for BLIMP1 (Minnich et al, 2016) and RIF1 at representative co-occupied BLIMP1 repressed targets from panel d.

273 **Discussion**

274

275 RIF1 has since long been shown to play a crucial role in humoral immunity because
276 of its ability to protect AID-induced DSBs at *Igh*, thus ensuring productive class
277 switching events [17–19]. Here, we describe a unexpected modulatory role of RIF1 in
278 regulating the timing of B cell differentiation to PCs.

279

280 Several recent studies have proposed that, besides SHM, BCR diversification *via*
281 CSR can also influence the differentiation outcome of GC B cells as well as the PC
282 transcriptome [56–61]. Given the strict dependency of CSR on RIF1[17–19] , it is tempting
283 to speculate that the skewed differentiation potential of RIF1-deficient B cells might
284 represent an indirect consequence of defective isotype switching. However, the *ex*
285 *vivo* recapitulation of the differentiation phenotype in the absence of RIF1 but not of
286 its downstream DNA end protection partner SHLD1 or of AID (Fig. 2), argues against
287 this possibility and in favor of a cell-intrinsic, DNA repair-independent role of RIF1 in
288 fine-tuning PC differentiation kinetics.

289

290 Our results support a model where RIF1 serves as a regulator of terminal B cell
291 differentiation through its capacity to counteract the premature repression of BLIMP1
292 target genes following activation. BLIMP1 is the master regulator of PC
293 differentiation [8,10,62]. Given that upregulation of BLIMP1 expression and appearance
294 of PCs are closely intertwined events, it might appear challenging to unambiguously
295 dissect the direct *versus* indirect aspects of RIF1 modulatory activity. However, the
296 substantial overlap of RIF1 occupancy at BLIMP1 targets that are also differentially
297 regulated in the absence of RIF1 is primarily observed at a subset of BLIMP1

298 repressed genes (Fig. 7). This finding indicates that RIF1 exerts its modulatory role
299 on PC differentiation by directly controlling the transcriptional status of these loci
300 rather than by indirectly influencing BLIMP1 expression. Mechanistically, the
301 dynamic regulation of RIF1 expression in mature B cells supports this gene
302 interaction co-regulatory model. We propose that high RIF1 levels prolong an active
303 B cell status to enable efficient *Igh* DSB repair and CSR whereas its down-regulation
304 contributes to a permissive environment for ASC differentiation (Fig. 1). Hence, our
305 study has uncovered the existence of a fine-tuning regulatory mechanism that
306 differentially impinges on the BLIMP1 transcriptional program controlling late B cell
307 differentiation.
308
309 Previous reports have highlighted RIF1's role in the differentiation of embryonic stem
310 cells [26,29,30,33]. In this context, RIF1 interacts with multiple Polycomb-group (PcG)
311 proteins, and alters chromatin accessibility and target gene expression [30,32,33].
312 Additionally, competition between RIF1 and KAP1 (and the long non-coding RNA
313 *Tsix*) for interaction with *Xist* promoters establishes the asymmetric X-chromosome
314 state at the onset of embryonic stem cell differentiation [32]. A similar gene binding
315 competition might apply to some of RIF1- and BLIMP1-co-occupied targets in the
316 context of activated B cells, suggesting a potentially widespread molecular
317 mechanism for RIF1-dependent transcriptional modulation across different cell types
318 and differentiation states.
319
320 The multifaceted role of RIF1 underscores the evolutionary ingenuity in repurposing
321 a single protein for diverse, yet equally critical, biological functions. RIF1
322 moonlighting in mature B cells has important implications for the pathological

consequences of deregulated plasma cell generation. Whilst producing a diverse Ig-switched repertoire enables effective antibody-mediated responses, tight regulation and fine tuning of late B cell differentiation is essential to counteract the development of autoimmunity and PC-derived malignancies [63–65]. Hence, by enabling *Igh* diversification *via* CSR while exerting a modulatory function on PC differentiation, RIF1 integrates key requirements for the establishment of protective humoral immunity.

330 **Methods**

331

332 **Mice and derived primary cell cultures**

333 *Rif1*$^{FH/FH}$ [44], *Cd19*$^{Cre}$ [66], *Rif1*$^{F/F}$*Cd19*$^{Cre/+}$ [18], *Shld1*$^{-/-}$ [67] and *Aicda*$^{-/-}$ [38] mice were

334 previously described and maintained on a C57BL/6 background. Mice were kept in a

335 specific pathogen-free (SPF) barrier facility and all experiments were performed in

336 compliance with the European Union (EU) directive 2010/63/EU, and in agreement

337 with Landesamt für Gesundheit und Soziales directives (LAGeSo, Berlin, Germany).

338 Mice of both genders were used for the experiments.

339 Resting B lymphocytes were isolated from mouse spleens using anti-CD43

340 MicroBeads (Miltenyi Biotec), and grown in RPMI 1640 medium (Life Technologies)

341 supplemented with 10% fetal bovine serum (FBS, Sigma-Aldrich), 10 mM HEPES

342 (Life Technologies), 1 mM Sodium Pyruvate (Life Technologies), 1X Antibiotic

343 Antimycotic (Life Technologies), 2 mM L-Glutamine (Life Technologies), and 1X 2-

344 Mercaptoethanol (Life Technologies) at 37 °C and 5% CO2 levels. Naïve B cells

345 were activated by addition of 5-25 μg/ml LPS (Sigma-Aldrich) and 5 ng/ml of mouse

346 recombinant IL-4 (Sigma-Aldrich) (L-I), or 5 μg/ml LPS, 10 ng/ml BAFF (PeproTech)

347 and 2 ng/ml TGFβ (L-B-T), or 5 μg/ml LPS only (L).

348

349 **Western Blot**

350 WB analysis of protein levels was performed on whole-cell lysates prepared by lysis

351 in radioimmunoprecipitation assay buffer (Sigma-Aldrich) supplemented with

352 Benzonase (Sigma-Aldrich), Complete EDTA free proteinase inhibitors (Roche) and

353 Pierce Phosphatase Inhibitor Mini Tablets (Thermo Fisher Scientific). The antibodies

354 used for WB analysis are anti-RIF1 [18] and anti-β-actin (Sigma).

355

356 **RNA-Seq**

357 For each RNA-Seq dataset, the analysis was performed on three mice per genotype.
358 Splenocytes were cultured in LPS and IL-4 (LI), LPS, BAFF and TGFβ (LBT), or LPS
359 (L), and cells were collected at the indicated time points by centrifugation. RNA was
360 extracted with TRIzol (Invitrogen) according to manufacturer's instructions, and
361 ribosomal RNA was depleted using Ribo-Zero Gold rRNA Removal Kit (Illumina) for
362 all datasets except for the RNA-Seq analysis in naïve versus LI/LBT/L-activated
363 splenocytes from WT mice (Fig. 1 and S1), for which RNase H (Epicentre) treatment
364 was used. Libraries were prepared with TruSeq Stranded Total RNA Library Prep Kit
365 Gold (Illumina), and run in one lane on a flow cell of NovaSeq 6000 SP (Illumina).

366

367 **ChIP-Seq**

368 ChIP-Seq for RIF1 in LPS and IL-4-stimulated splenocyte cultures was previously
369 described [25]. H3K4me3 ChIP-Seq was performed in splenocytes activated with LPS
370 and IL-4 for 72 h, and employed anti-H3K4me3 antibody (abcam, ab8580) for the
371 ChIP part of the previously described protocol [68]. For H3K27me3 ChIP-Seq, we used
372 H3K27me3 antibody (Cell Signalling, C36B11), and 2.5% human shared chromatin
373 was spiked into all samples as an internal reference for normalization [69].

374

375 **B cell proliferation, development and differentiation analyses**

376 For analysis of CSR in *ex vivo* cultures, cell suspensions were stained with anti-
377 IgG1-APC (BD Biosciences), anti-IgG3-Biotin and Streptavidin-APC (BD
378 Biosciences), or anti-IgG2b-PE (BioLegend). For analysis of plasmablast
379 differentiation *ex vivo*, isolated naïve splenic B cells were cultured at a density of 0,5

380 x $10^6$ cells/ml in the presence of 25 μg/ml LPS and 5 ng/ml IL-4 and stained with
381 anti-CD138 (BioLegend). B cell proliferation was assessed by CellTrace Violet
382 (Thermofisher) dilution according to manufacturer's instructions. For analysis of
383 plasma cell-like differentiation *ex vivo*, the induced GC B (iGB) culture system was
384 used as described before [35,36]. Briefly, 40LB feeder cells (Balb/c 3T3 cell line
385 expressing exogenous CD40-ligand (CD40L) and B-cell activating factor (BAFF))
386 were irradiated with 80 Gy and co-cultured with primary splenic B cells for 4 days in
387 high glucose DMEM medium (Gibco) supplemented with 10% FBS, 10 mM HEPES,
388 1 mM Sodium Pyruvate, 1X Pen/Strep (Life Technologies), 1x MEM Non-Essential
389 Amino Acids (Life Technologies), 2 mM L-Glutamine, 1X 2-Mercaptoethanol and 1
390 ng/ml IL-4 at 37 °C and 5% $CO_2$ levels. On day 4, cells were harvested, washed one
391 time with PBS and re-plated in a newly irradiated 40LB feeder layer in the presence
392 of 10 ng/ml IL-21 (PeproTech) for the next 4 days. For assessing CSR and plasma
393 cell-like differentiation on day 4 and 8, 1 x $10^6$ B cells were washed one time with
394 FACS buffer (PBS supplemented with 1% FCS and 1 mM EDTA), blocked with
395 TruStain fcX (BioLegend) for 10 min at 4° C and stained with the respective
396 antibodies as stated above. 1 µg/ml of propidium iodide (PI) was used for live/dead
397 cell staining.
398 For analysis of germinal centers and plasma cell compartments *in vivo*, 8-14 week-
399 old mice were sacrificed to isolate the spleen, tibia, and Payer's patches (PP). Single
400 cell suspensions from spleen and tibia were incubated for 2 min with ACK buffer
401 (Gibco) for red blood cell lysis. For surface staining, 5-7 × $10^6$ cells were first blocked
402 with TruStain fcX for 10 min at 4 °C and then stained for 20 min at 4° C. The
403 antibodies employed for the staining were detecting: CD138, CD267/ TACI (BD
404 Pharmingen), MHC-II (Biolegend) and CD93/AA4.1 (Biolegend) for the plasma cell

405 compartment; CD19, B220, CD86 (Biolegend), CD184/CXCR4, CD95/FAS (BD
406 Pharmingen), IgA and CD38 (eBioscience) for PP analysis; and CD19, B220, CD38,
407 CD95/FAS and IgG1 (BD Bioscience) for splenic GC analysis. Cells were
408 resuspended in FACS buffer containing PI and analyzed. Immunization was
409 performed by intraperitoneal injection of 100 µg of NP-CGG (Biosearch
410 Technologies; ratio 10-20) precipitated in alum (Sigma).
411 All samples were acquired on a LSRFortessa cell analyzer (BD Biosciences).
412
413 **ELISpot assay**
414 To detect NP-specific plasma cells, MultiScreen$_{HTS}$-IP plates (Merck) were activated
415 with 35% ethanol in PBS, washed three times with PBS, and finally coated with 2
416 µg/mL NP-BSA (loading ratio >20, BioCat) at 4°C overnight. Next day, plates were
417 washed twice with PBS and blocked with ELISpot medium (RPMI 1640
418 supplemented with 10% FBS and 1% pen/strep) for 2 h at 37 °C. 5 x $10^6$ total spleen
419 and BM cells (as well as serial five-fold dilutions) were added to the NP-BSA coated
420 plates and cultured overnight in ELISpot medium. The following day, wells were
421 washed six times with PBS supplemented with 0.1 % Tween20 and incubated for 2 h
422 with 1 µg/mL biotinylated goat α-mouse IgM or IgG1 (SouthernBiotech) at 37 °C.
423 Spot visualization was performed by incubation with 0.3 U/ml streptavidin-AP
424 conjugate (Roche) for 30 min at room temperature followed by three washes with
425 running distilled water, equilibration in AP buffer (100 mM Tris-HCl, pH 9.0, 150 mM
426 NaCl, and 1 mM $MgCl_2$), and development using NBT/BCIP substrate mix (Promega)
427 diluted in AP buffer. Plates were scanned and spots were counted using the
428 ImmunoSpot® Series 6 Alfa Analyzer and ImmunoCapture™ Image Acquisition as
429 well as ImmunoSpot® Analysis software (C.T.L.).

430

431 **Data availability**

432 All RNA-Seq datasets reported in this study, and H3K4me3 and H3K27me3 ChIP-
433 Seq data have been deposited in the GEO repository under accession number
434 GSE237560. The transcriptional signatures of activated B cells, PBs, and PCs have
435 been defined using the corresponding (and naïve B cells for baseline comparison)
436 RNA-Seq datasets from ([10], GSE71698). RIF1 ChIP-Seq was previously reported ([25],
437 GSE228880). The BLIMP1-bound regions in activated B cells were defined based on
438 the BLIMP1 Bio-ID dataset from ([10], GSE71698). The lists of BLIMP1-activated and -
439 repressed targets have been previously described [10].

440

441 **Data analysis and Softwares**

442 *RNA-Seq.* All RNA-Seq datasets, whether specifically generated for this study or
443 obtained from public databases, have been analyzed/re-analyzed using the same
444 pipeline implemented for this project. The RNA-seq data was analyzed using the
445 Galaxy platform [70]. HTSeq [71] mapped the reads to the GRCm38 assembly for mouse
446 and GENCODE-M25 (www.gencodegenes.org) was used to count the transcript
447 abundance. Differential expression analysis was done *via* the DESeq2 [72] package
448 for R, which uses the Wald test for significance. To define the transcriptional
449 signatures of activated B cells, PBs, and PCs, the analysis was performed using the
450 naïve B cell RNA-Seq dataset from the same study [10] for baseline comparison.
451 Expression of differentially expressed genes were obtained from Immgen database
452 [34] and visualize by R and ggolot2 packages (https://ggplot2.tidyverse.org/) after
453 scaling. For the comparative assessment of $Cd19^{Cre/+}$ and $Rif1^{F/F}Cd19^{Cre/+}$ B cell
454 transcriptomes at 48 h after activation, RNA-seq datasets from L-I and L-B-T

455 splenocytes cultures were merged. The increase in sample size (from 3 to 6 repeats)
456 for both groups enhanced statistical power to detect minor gene expression
457 differences. The multiple treatments are used to discern genotype effects, thus
458 ensuring that the observed differences are due to the absence of RIF1.
459 *ChIP-Seq.* ChIP-Seq and BLIMP1 Bio-ID datasets have been analyzed/re-analyzed
460 using the same pipeline implemented for this project. FASTQ files were aligned
461 against mouse genome (mm10) using BWA aligner [73]. Processing and peak-calling
462 of ChIP-Seq data were performed with MACS2 [74]. Peak annotation was done using
463 R and ChIPseeker package [75]. Functional assessment of genomic regions
464 enrichment and motif analysis were performed by GREAT and MEME-ChIP,
465 respectively [45,76]. For the comparative genomic distribution analysis of RIF1,
466 H3K4me3, and H3K27me3 in reference to BLIMP1-occupied regions, the aligned
467 reads were converted into BigWig format. The signals were subsequently
468 transformed into a matrix *via* the ComputeMatrix software, and visualized as a
469 heatmap[77].
470 *Statistical analysis.* The statistical significance of differences between groups was
471 determined by the Mann–Whitney U test for all data presented in this study, with the
472 following exceptions. For the RNA-Seq analysis, the expression values of specific
473 transcripts were normalized by DESeq2, and genes with an adjusted p-value $< 0.05$
474 were considered to be significantly differentially expressed. Statistical details of
475 experiments can be also found in the figure legends.
476 *Hypergeometric analysis.* Gene expression data were sourced from experiments
477 from this study and published datasets[10] (GSE71698) and compiled into a single CSV
478 in parallel to a universe of genes (list of all known genes in mouse genome, mm10).
479 A custom R function was developed to conduct overrepresentation analysis *via*

hypergeometric testing. This function computes the likelihood of observing the intersection of genes between two lists, considering the total gene count in the universe and adjusting for the sizes of the lists involved. Pairwise comparisons between all unique pairs of gene lists were conducted by the hypergeometric test, which was implemented using the phyper function from R's base stats package, with the test's directionality set to identify overrepresented genes. The resulting p-values were adjusted for multiple comparisons using the Bonferroni correction method to control for the family-wise error rate. For a comprehensive overview of the pairwise comparison results, we reported the Bonferroni-adjusted p-values as -log10 values. This transformation enhances the interpretability of the results, with higher values indicating more significant overlaps between gene list pairs.

*Source Codes for Data Analysis.* All codes used to generate graphs and to compare different datasets can be found on our GitHub page (https://github.com/arahjou/RIF1_paper.git).

**Acknowledgments**

We thank all members of the Di Virgilio lab for discussion; L. Keller and T. Rüster (Di Virgilio lab, MDC, Berlin) for genotyping; W. Winkler and C. Farre i Diaz (Janz/Mathas and K. Rajewsky labs, MDC) for *in vivo* and ELISpot protocols; and D. Pasini (IEO, Milan) and G. Gargiulo (MDC) for their valuable feedback. Figure schematics were created using images from BioRender. The project was funded by the Helmholtz-Gemeinschaft Zukunftsthema "Immunology and Inflammation" ZT-0027 (to M.D.V.) and the Initiative and Networking Fund of the Helmholtz Association (to M.D.V.).

**Author contributions**

A.R. and E.K. conceived the project idea, designed and performed experiments; M.B.L. and V.D.B prepared the RNA-seq libraries; A.R. analyzed all high-throughput sequencing data; R.A. contributed to the sequencing data analysis; R.P. engaged in active discussions on the study; M.D.V. secured the funding for the project, supervised all aspects of the study, and wrote the manuscript; A.R. and E.K. reviewed and edited the manuscript.

**Competing interests**

The authors declare no competing interests.

## References


514 1. Lin, S. G., Ba, Z., Alt, F. W. & Zhang, Y. Chapter Three - RAG Chromatin
515 Scanning During V(D)J Recombination and Chromatin Loop Extrusion are
516 Related Processes. in *Advances in Immunology* (ed. Alt, F.) vol. 139 93–135
517 (Academic Press, 2018).
518 2. Nemazee, D. Mechanisms of central tolerance for B cells. *Nat Rev Immunol* **17**,
519 281–294 (2017).
520 3. Chandra, V., Bortnick, A. & Murre, C. AID Targeting: Old Mysteries and New
521 Challenges. *Trends Immunol* **36**, 527–535 (2015).
522 4. Methot, S. P. & Di Noia, J. M. Molecular Mechanisms of Somatic Hypermutation
523 and Class Switch Recombination. *Adv Immunol* **133**, 37–87 (2017).
524 5. Victora, G. D. & Nussenzweig, M. C. Germinal Centers. *Annual Review of*
525 *Immunology* **40**, 413–442 (2022).
526 6. Elsner, R. A. & Shlomchik, M. J. Germinal Center and Extrafollicular B Cell
527 Responses in Vaccination, Immunity, and Autoimmunity. *Immunity* **53**, 1136–
528 1150 (2020).
529 7. Nutt, S. L., Fairfax, K. A. & Kallies, A. BLIMP1 guides the fate of effector B and T
530 cells. *Nat Rev Immunol* **7**, 923–927 (2007).
531 8. Kallies, A. *et al.* Initiation of Plasma-Cell Differentiation Is Independent of the
532 Transcription Factor Blimp-1. *Immunity* **26**, 555–566 (2007).
533 9. Shaffer, A. L., Rosenwald, A. & Staudt, L. M. Lymphoid Malignancies: the dark
534 side of B-cell differentiation. *Nat Rev Immunol* **2**, 920–933 (2002).
535 10. Minnich, M. *et al.* Multifunctional role of the transcription factor Blimp-1 in
536 coordinating plasma cell differentiation. *Nat Immunol* **17**, 331–343 (2016).

537 11. Tellier, J. *et al.* Blimp-1 controls plasma cell function through the regulation of
538 immunoglobulin secretion and the unfolded protein response. *Nat Immunol* **17**,
539 323–330 (2016).
540 12. Hardy, C. F., Sussel, L. & Shore, D. A RAP1-interacting protein involved in
541 transcriptional silencing and telomere length regulation. *Genes Dev.* **6**, 801–814
542 (1992).
543 13. Ray Chaudhuri, A. *et al.* Replication fork stability confers chemoresistance in
544 BRCA-deficient cells. *Nature* **535**, 382–387 (2016).
545 14. Garzón, J., Ursich, S., Lopes, M., Hiraga, S. & Donaldson, A. D. Human RIF1-
546 Protein Phosphatase 1 Prevents Degradation and Breakage of Nascent DNA on
547 Replication Stalling. *Cell Reports* **27**, 2558-2566.e4 (2019).
548 15. Mukherjee, C. *et al.* RIF1 promotes replication fork protection and efficient restart
549 to maintain genome stability. *Nat Commun* **10**, 3287 (2019).
550 16. Balasubramanian, S. *et al.* Protection of nascent DNA at stalled replication forks
551 is mediated by phosphorylation of RIF1 intrinsically disordered region. *eLife* **11**,
552 e75047 (2022).
553 17. Chapman, J. R. *et al.* RIF1 Is Essential for 53BP1-Dependent Nonhomologous
554 End Joining and Suppression of DNA Double-Strand Break Resection. *Molecular*
555 *Cell* **49**, 858 (2013).
556 18. Di Virgilio, M. *et al.* Rif1 Prevents Resection of DNA Breaks and Promotes
557 Immunoglobulin Class Switching. *Science* **339**, 10.1126/science.1230624 (2013).
558 19. Escribano-Díaz, C. *et al.* A Cell Cycle-Dependent Regulatory Circuit Composed
559 of 53BP1-RIF1 and BRCA1-CtIP Controls DNA Repair Pathway Choice.
560 *Molecular Cell* **49**, 872–883 (2013).

561 20. Feng, L., Fong, K.-W., Wang, J., Wang, W. & Chen, J. RIF1 Counteracts BRCA1-
562 mediated End Resection during DNA Repair *. *Journal of Biological Chemistry*
563 **288**, 11135–11143 (2013).
564 21. Zimmermann, M., Lottersberger, F., Buonomo, S. B., Sfeir, A. & De Lange, T.
565 53BP1 Regulates DSB Repair Using Rif1 to Control 5′ End Resection. *Science*
566 **339**, 700–704 (2013).
567 22. Yamazaki, S. *et al.* Rif1 regulates the replication timing domains on the human
568 genome. *EMBO J* **31**, 3667–3677 (2012).
569 23. Foti, R. *et al.* Nuclear Architecture Organized by Rif1 Underpins the Replication-
570 Timing Program. *Mol Cell* **61**, 260–273 (2016).
571 24. Gnan, S. *et al.* Nuclear organisation and replication timing are coupled through
572 RIF1–PP1 interaction. *Nat Commun* **12**, 2910 (2021).
573 25. Malzl, D. *et al. RIF1 Regulates Replication Origin Activity and Early Replication*
574 *Timing in B Cells*. http://biorxiv.org/lookup/doi/10.1101/2023.03.31.535086 (2023)
575 doi:10.1101/2023.03.31.535086.
576 26. Dan, J. *et al.* Rif1 maintains telomere length homeostasis of ESCs by mediating
577 heterochromatin silencing. *Dev Cell* **29**, 7–19 (2014).
578 27. Liu, C. *et al.* Rif1 Regulates Self-Renewal and Impedes Mesendodermal
579 Differentiation of Mouse Embryonic Stem Cells. *Stem Cell Rev Rep* (2023)
580 doi:10.1007/s12015-023-10525-1.
581 28. Zhang, W. *et al.* Rif1 and Hmgn3 regulate the conversion of murine trophoblast
582 stem cells. *Cell Rep* **38**, 110570 (2022).
583 29. Li, P., Ma, X., Adams, I. R. & Yuan, P. A tight control of Rif1 by Oct4 and Smad3
584 is critical for mouse embryonic stem cell stability. *Cell Death Dis* **6**, e1588 (2015).

585 30. Li, L. *et al.* Rif1 interacts with non-canonical polycomb repressive complex
586 PRC1.6 to regulate mouse embryonic stem cells fate potential. *Cell Regen* **11**, 25
587 (2022).
588 31. Saha, T., Sundaravinayagam, D. & Di Virgilio, M. Charting a DNA Repair
589 Roadmap for Immunoglobulin Class Switch Recombination. *Trends Biochem Sci*
590 **46**, 184–199 (2021).
591 32. Enervald, E. *et al.* RIF1 and KAP1 differentially regulate the choice of inactive
592 versus active X chromosomes. *The EMBO Journal* **40**, e105862 (2021).
593 33. Rodriguez-Terrones, D. *et al.* A molecular roadmap for the emergence of early-
594 embryonic-like cells in culture. *Nat Genet* **50**, 106–119 (2018).
595 34. The Immunological Genome Project *et al.* ImmGen at 15. *Nat Immunol* **21**, 700–
596 703 (2020).
597 35. Haniuda, K. & Kitamura, D. Induced Germinal Center B Cell Culture System. *Bio*
598 *Protoc* **9**, e3163 (2019).
599 36. Nojima, T. *et al.* In-vitro derived germinal centre B cells differentially generate
600 memory B or plasma cells in vivo. *Nature Communications 2011 2:1* **2**, 1–11
601 (2011).
602 37. Reboldi, A. *et al.* IgA production requires B cell interaction with subepithelial
603 dendritic cells in Peyer's patches. *Science* **352**, aaf4822 (2016).
604 38. Muramatsu, M. *et al.* Class switch recombination and hypermutation require
605 activation-induced cytidine deaminase (AID), a potential RNA editing enzyme.
606 *Cell* **102**, 553–563 (2000).
607 39. Zaheen, A. *et al.* AID constrains germinal center size by rendering B cells
608 susceptible to apoptosis. *Blood* **114**, 547–554 (2009).

609 40. Boulianne, B. *et al.* AID and caspase 8 shape the germinal center response
610 through apoptosis. *J Immunol* **191**, 5840–5847 (2013).
611 41. Mayer, C. T. *et al.* The microanatomic segregation of selection by apoptosis in
612 the germinal center. *Science* **358**, eaao2602 (2017).
613 42. Enervald, E. *et al.* RIF1 and KAP1 differentially regulate the choice of inactive
614 versus active X chromosomes. *The EMBO Journal* **40**, e105862 (2021).
615 43. Shi, W. *et al.* Transcriptional profiling of mouse B cell terminal differentiation
616 defines a signature for antibody-secreting plasma cells. *Nat Immunol* **16**, 663–
617 673 (2015).
618 44. Cornacchia, D. *et al.* Mouse Rif1 is a key regulator of the replication-timing
619 programme in mammalian cells. *The EMBO Journal* **31**, 3678–3690 (2012).
620 45. McLean, C. Y. *et al.* GREAT improves functional interpretation of cis-regulatory
621 regions. *Nat Biotechnol* **28**, 495–501 (2010).
622 46. Babushku, T. *et al.* Notch2 controls developmental fate choices between
623 germinal center and marginal zone B cells upon immunization. *Nat Commun* **15**,
624 1960 (2024).
625 47. Gloury, R. *et al.* Dynamic changes in Id3 and E-protein activity orchestrate
626 germinal center and plasma cell development. *J Exp Med* **213**, 1095–1111
627 (2016).
628 48. Bönelt, P. *et al.* Precocious expression of Blimp1 in B cells causes autoimmune
629 disease with increased self-reactive plasma cells. *The EMBO Journal* **38**,
630 e100010 (2019).
631 49. Guo, M. *et al.* EZH2 Represses the B Cell Transcriptional Program and
632 Regulates Antibody-Secreting Cell Metabolism and Antibody Production. *J*
633 *Immunol* **200**, 1039–1052 (2018).

634 50. Mlynarczyk, C. *et al.* BTG1 mutation yields supercompetitive B cells primed for
635 malignant transformation. *Science* **379**, eabj7412 (2023).
636 51. Hargreaves, D. C. *et al.* A Coordinated Change in Chemokine Responsiveness
637 Guides Plasma Cell Movements. *Journal of Experimental Medicine* **194**, 45–56
638 (2001).
639 52. Wehrli, N. *et al.* Changing responsiveness to chemokines allows medullary
640 plasmablasts to leave lymph nodes. *European Journal of Immunology* **31**, 609–
641 616 (2001).
642 53. Andreani, V. *et al.* Cochaperone Mzb1 is a key effector of Blimp1 in plasma cell
643 differentiation and β1-integrin function. *Proceedings of the National Academy of*
644 *Sciences* **115**, E9630–E9639 (2018).
645 54. Fang, D.-F. *et al.* NEDD4 ubiquitinates TRAF3 to promote CD40-mediated AKT
646 activation. *Nat Commun* **5**, 4513 (2014).
647 55. Hofmann, K., Clauder, A.-K. & Manz, R. A. Targeting B Cells and Plasma Cells in
648 Autoimmune Diseases. *Front. Immunol.* **9**, (2018).
649 56. Gómez-Escolar, C. *et al.* Single cell clonal analysis identifies an AID -dependent
650 pathway of plasma cell differentiation. *EMBO Reports* **23**, e55000 (2022).
651 57. Kometani, K. *et al.* Repression of the Transcription Factor Bach2 Contributes to
652 Predisposition of IgG1 Memory B Cells toward Plasma Cell Differentiation.
653 *Immunity* **39**, 136–147 (2013).
654 58. Gitlin, A. D. *et al.* Independent Roles of Switching and Hypermutation in the
655 Development and Persistence of B Lymphocyte Memory. *Immunity* **44**, 769–781
656 (2016).

657 59. King, H. W. *et al.* Single-cell analysis of human B cell maturation predicts how
658 antibody class switching shapes selection dynamics. *Sci Immunol* **6**, eabe6291
659 (2021).
660 60. Higgins, B. W., McHeyzer-Williams, L. J. & McHeyzer-Williams, M. G.
661 Programming Isotype-Specific Plasma Cell Function. *Trends in Immunology* **40**,
662 345–357 (2019).
663 61. Higgins, B. W. *et al.* Isotype-specific plasma cells express divergent
664 transcriptional programs. *Proceedings of the National Academy of Sciences* **119**,
665 e2121260119 (2022).
666 62. Fairfax, K. A. *et al.* Different Kinetics of Blimp-1 Induction in B Cell Subsets
667 Revealed by Reporter Gene. *The Journal of Immunology* **178**, 4104–4111
668 (2007).
669 63. Elkon, K. & Casali, P. Nature and functions of autoantibodies. *Nat Clin Pract*
670 *Rheumatol* **4**, 491–498 (2008).
671 64. Barwick, B. G., Gupta, V. A., Vertino, P. M. & Boise, L. H. Cell of Origin and
672 Genetic Alterations in the Pathogenesis of Multiple Myeloma. *Front Immunol* **10**,
673 1121 (2019).
674 65. García-Sanz, R. *et al.* Origin of Waldenstrom's macroglobulinaemia. *Best Pract*
675 *Res Clin Haematol* **29**, 136–147 (2016).
676 66. Rickert, R. C., Roes, J. & Rajewsky, K. B lymphocyte-specific, Cre-mediated
677 mutagenesis in mice. *Nucleic Acids Res* **25**, 1317–1318 (1997).
678 67. Vincendeau, E. *et al.* SHLD1 is dispensable for 53BP1-dependent V(D)J
679 recombination but critical for productive class switch recombination. *Nat*
680 *Commun* **13**, 3707 (2022).

681 68. Pavri, R. *et al.* Activation-Induced Cytidine Deaminase Targets DNA at Sites of
682 RNA Polymerase II Stalling by Interaction with Spt5. *Cell* **143**, 122–133 (2010).
683 69. Bonhoure, N. *et al.* Quantifying ChIP-seq data: a spiking method providing an
684 internal reference for sample-to-sample normalization. *Genome Res.* **24**, 1157–
685 1168 (2014).
686 70. The Galaxy Community *et al.* The Galaxy platform for accessible, reproducible
687 and collaborative biomedical analyses: 2022 update. *Nucleic Acids Research* **50**,
688 W345–W351 (2022).
689 71. Anders, S., Pyl, P. T. & Huber, W. HTSeq--a Python framework to work with high-
690 throughput sequencing data. *Bioinformatics* **31**, 166–169 (2015).
691 72. Love, M. I., Huber, W. & Anders, S. Moderated estimation of fold change and
692 dispersion for RNA-seq data with DESeq2. *Genome Biol* **15**, 550 (2014).
693 73. Li, H. & Durbin, R. Fast and accurate short read alignment with Burrows-Wheeler
694 transform. *Bioinformatics* **25**, 1754–1760 (2009).
695 74. Zhang, Y. *et al.* Model-based Analysis of ChIP-Seq (MACS). *Genome Biol* **9**,
696 R137 (2008).
697 75. Yu, G., Wang, L.-G. & He, Q.-Y. ChIPseeker: an R/Bioconductor package for
698 ChIP peak annotation, comparison and visualization. *Bioinformatics* **31**, 2382–
699 2383 (2015).
700 76. Machanick, P. & Bailey, T. L. MEME-ChIP: motif analysis of large DNA datasets.
701 *Bioinformatics* **27**, 1696–1697 (2011).
702 77. Ramírez, F. *et al.* deepTools2: a next generation web server for deep-sequencing
703 data analysis. *Nucleic Acids Res* **44**, W160-165 (2016).
704 78. Dunn, O. J. Multiple Comparisons among Means. *Journal of the American*
705 *Statistical Association* **56**, 52–64 (1961).

## Additional information

## Supplemental information:

**Supplemental Figure 1**

**Stimulation-dependent clustering of B cell transcriptomics profiles after *ex vivo* activation.** Related to Figure 1.

**Supplemental Figure 2**

**RIF1 deficiency results in a reduced number of class-switched GC B cells upon immunization.** Related to Figure 3.

**Supplemental Figure 3**

**RIF1 ablation does not result in detectable changes of the plasma cell compartment in steady state condition.** Related to Figure 3.

**Supplemental Figure 4**

**RIF1 deficiency alters the transcriptional landscape of activated B cells.** Related to Figure 5.

**Supplemental Table 1**

**Pairwise comparison of differentially regulated genes in control (*Cd19*$^{Cre/+}$) *versus Rif1*$^{F/F}$*Cd19*$^{Cre/+}$ splenocytes.** Related to Figures 5 and S4.

**Supplemental Table 2**

**Lists of genes in the PB and PC transcriptional signatures that are differentially regulated in *Rif1*$^{F/F}$*Cd19*$^{Cre/+}$ activated B cells.** Related to Figure 5.

**Supplemental Table 3**

**Lists of RIF1-bound genes in the top GREAT gene ontology enrichment categories.** Related to Figure 6.

**Supplemental Table 4**

**Lists of RIF1&BLIMP1 target genes.** Related to Figure 7.